

## SINGLE-CRYSTAL XRD, TEM, AND THERMAL STUDIES OF THE SATELLITE REFLECTIONS IN NEPHELINE

ISHMAEL HASSAN<sup>§</sup>

*Department of Chemistry, University of the West Indies, Mona, Kingston 7, Jamaica*

SYTLE M. ANTAO

*Mineral Physics Institute and Department of Geosciences, State University of New York, Stony Brook,  
New York 11794-2100, U.S.A.*

AHMED A.M. HERSI

*Department of Earth and Environmental Sciences, University of Kuwait, P.O. Box 5969, Safat, 13060, Kuwait*

### ABSTRACT

A sample of nepheline from Egan Chute, near Bancroft, Ontario, with a chemical composition  $(K_{1.32}\square_{0.68})(Na_{6.05}Ca_{0.22})[Al_{7.77}Si_{8.21}O_{32}]$ , has been studied using single-crystal X-ray diffraction, transmission electron microscopy (TEM), thermal analyses, and powder X-ray diffraction. Its structure was refined in space group  $P6_3$  to an  $R_1$  index of 0.041 on the basis of 737 unique observed reflections. The parameters of the pseudo-hexagonal subcell are  $a$  9.9853(7),  $c$  8.3689(17) Å. The Al and Si atoms are fully ordered. The O1 framework oxygen atom is disordered over three nearby positions that are slightly displaced off the three-fold axis in the average structure. Vacancies are present at the K site. Selected-area electron diffraction (SAED) patterns show that the satellite reflections are very weak and diffuse, and give rise to an incommensurate supercell. Images obtained by high-resolution transmission electron microscopy (HRTEM) indicate that nepheline probably consists of domains that are separated by possible antiphase boundaries (APBs). Results from thermal analyses indicate that a displacive transformation occurs in nepheline at 292°C and represents a positional order–disorder of O1 oxygen atoms. A K –  $\square$  order–disorder transformation occurs at 399°C and is attributed to disordering of K ions and  $\square$  vacancies in the large sixfold channels of the nepheline structure. An Al–Si order–disorder transformation occurs at 963°C and involves the highest energy among the various transitions. The ordering that gives rise to the satellite reflections is destroyed in the electron beam and results in twinned unit-cells.

*Keywords:* nepheline, crystal structure, superstructure, single-crystal X-ray diffraction, transmission electron microscopy, thermal analyses, phase transitions, Egan Chute, Bancroft, Ontario.

### SOMMAIRE

Nous avons caractérisé un échantillon de néphéline provenant de Egan Chute, près de Bancroft, en Ontario, ayant une composition  $(K_{1.32}\square_{0.68})(Na_{6.05}Ca_{0.22})[Al_{7.77}Si_{8.21}O_{32}]$ , par diffraction X sur monocristal, microscopie électronique à transmission, analyses thermiques, et diffraction X sur poudre. Nous en avons affiné la structure dans le groupe spatial  $P6_3$  jusqu'à un résidu  $R_1$  de 0.041 en nous servant de 737 réflexions uniques observées. Les paramètres de la sous-maille pseudo-hexagonale sont  $a$  9.9853(7),  $c$  8.3689(17) Å. Les atomes Al et Si sont complètement ordonnés. L'atome d'oxygène O1 de la trame est déplacé sur trois positions par rapport à la position idéale sur l'axe de symétrie 3, ce qui provoque un désordre de position. Des lacunes sont présentes au site K. Les tracés de diffraction électronique sur aire réduite montrent que les réflexions satellites sont de très faible intensité et floues, et mènent à la définition d'une surmaille incommensurable. Les images obtenues en haute résolution par microscopie électronique à transmission indiquent que la néphéline de Egan Chute contient probablement des domaines séparés l'un de l'autre par des interfaces antiphassées. Les résultats de l'analyse thermique indiquent la présence d'une transition due à un déplacement d'atomes à 292°C, attribuable à une relation ordre–désordre dans la position de l'atome O1. Une transformation ordre–désordre due à K et  $\square$  a lieu à 399°C et serait attribuable au désordre qui intervient parmi les ions de K et les lacunes dans les canaux à axe de symétrie 6 dans la structure. Une transformation ordre–désordre affecte la distribution de Al et Si à 963°C et

<sup>§</sup> E-mail address: ishmael.hassan@uwimona.edu.jm

requiert la plus grande énergie de toutes les transitions. La mise en ordre qui cause les réflexions satellites est détruite dans le faisceau d'électrons et mène à la formation de mailles élémentaires maclées.

(Traduit par la Rédaction)

*Mots-clés:* néphéline, structure cristalline, surstructure, diffraction X sur monocristal, microscopie électronique à transmission, analyses thermiques, transitions de phase, Egan Chute, Bancroft, Ontario.

## INTRODUCTION

Nepheline, ideally  $\text{Na}_3\text{K}[\text{Al}_4\text{Si}_4\text{O}_{16}]$ , is an important rock-forming mineral that has wide occurrences in many silica-poor alkaline igneous rocks and associated pegmatites. Natural examples of nepheline are intermediate members of a solid solution that extends from  $\text{Na}[\text{AlSiO}_4]$  to  $\text{K}[\text{AlSiO}_4]$  (kalsilite). Nepheline and kalsilite are not isostructural, but both structures have a tridymite-type framework. Both nepheline and kalsilite have been the subjects of several studies (*e.g.*, Sahama 1958, McConnell 1991, Capobianco & Carpenter 1989, Carpenter & Cellai 1996, Xu & Veblen 1996).

Satellite reflections occur in nepheline samples from various localities and origins (Sahama 1958, 1962, McConnell 1962, 1981, 1991). In different specimens, the satellite reflections show a wide range of character with respect to intensity and sharpness. The positions of the satellite reflections in three specimens were defined in reciprocal space in terms of the reciprocal cell by vector coordinates  $\pm (\frac{1}{3}, \frac{1}{3}, \pm z)$ , with  $z$  equal to 0.2068, 0.2058, and 0.2134 (McConnell 1962). The satellite reflections in nepheline indicate that the structure is ordered in a superstructure with the supercell defined as  $a_s = a\sqrt{3}$ , whereas in the  $c$  direction the structure is modulated with an incommensurate wavelength. Various models have been proposed for the nepheline supercell (McConnell 1962, 1981, 1991, Parker & McConnell 1971, Parker 1972, Merlini 1984, Hayward *et al.* 2000).

We have studied the satellite reflections in nepheline using single-crystal X-ray diffraction, high-resolution transmission electron microscopy (HRTEM), selected-area electron diffraction (SAED) patterns, high-temperature powder X-ray diffraction, and thermal analyses (TG, DTA, and DSC). Our aim is to establish a well-refined structural model, which may then be used to explain the formation of the superstructures in nepheline.

## REVIEW OF THE CRYSTAL STRUCTURE OF NEPHELINE

Structures of nepheline have been refined for specimens from various geological origins: a moderate-temperature nepheline from a gneiss from Bancroft, Ontario (Foreman & Peacor 1970), a plutonic specimen from Larvik, Norway (Dollase 1970) and its Na-exchanged derivative (Dollase & Peacor 1971), a volcanic specimen from Monte Somma, Italy (Simmons & Peacor

1972), K-deficient nepheline synthesized hydrothermally (Dollase & Thomas 1978), and Na-rich nepheline synthesized hydrothermally (Gregorkiewitz 1984). Recently, the crystal structures of three samples of nepheline of different origins were refined by Tait *et al.* (2003). The structure of an AlGe analogue of nepheline is also available (Hammond & Barbier 1998). The crystal structures of aluminosilicate nepheline were reviewed by Merlini (1984). Comparisons of structural data on nepheline indicate structural differences such as Al–Si distribution on the one hand, and K, Na, and vacancy distribution on the other, which suggest that the differences may be a function of composition, growth conditions, or thermal history. These relationships are of interest because of their geological implications, but their exact nature is still unknown because of the difficulties that have been encountered during the final stages of most previous structural refinements of nepheline (Gregorkiewitz 1984). Note, however, that Tait *et al.* (2003) encountered no such difficulties.

The structure of nepheline is a stuffed derivative of tridymite with approximately half the Si atoms replaced by Al, and with Na and K as interstitial charge-balancing cations (Schiebold 1930, Buerger *et al.* 1954, Hahn & Buerger 1955). The structure of nepheline consists of four independent tetrahedra ( $T = \text{Al}$  or  $\text{Si}$ ) per unit cell (Fig. 1). The  $T_1$  and  $T_2$  sites occupy special positions on the three-fold axes, and  $T_3$  and  $T_4$  occupy general positions. The apices of the tetrahedra occupied by  $T_1$  and  $T_4$  cations are arranged in one direction along the  $c$  axis, and those occupied by  $T_2$  and  $T_3$  point in the opposite direction. The cavities in the framework are too large for the alkali atoms, in particular the smaller Na atom, to occupy their centers and still maintain proper bonding to the framework oxygen atoms located in the channel walls. Therefore, the framework is distorted by rotation of the framework tetrahedra about the hexagonal axis, such that the apical oxygen atoms, O1, are distributed slightly off the threefold axis toward one of the three neighboring Na atoms (Fig. 1). Each O1 atom has a site occupancy of  $\frac{1}{3}$ . In nepheline, two of the six-membered rings are hexagonal, and six are oval-shaped. Ideally, the Na atoms fully occupy six small oval-shaped  $B$  cavities, and the K atoms occupy two large hexagonal  $A$  cavities, thus giving  $\text{Na}_6\text{K}_2[\text{Al}_8\text{Si}_8\text{O}_{32}]$  as an ideal composition for nepheline.

Al and Si are ordered over the tetrahedral sites in nepheline. In general, the  $T_1$  and  $T_4$  sites are Al-rich, and the  $T_2$  and  $T_3$  sites are Si-rich. The  $T_1$ – $T_2$  pair is

bonded to the positionally disordered O1 atoms, whereas the  $T_3$ – $T_4$  pair is not. In addition, the  $T_1$  and  $T_2$  tetrahedra are surrounded by only Na atoms ( $B$  sites), whereas the  $T_3$  and  $T_4$  tetrahedra are surrounded by A and  $B$  sites (Fig. 1).

#### EXPERIMENTAL

The nepheline sample used in this study is from Egan Chute on the York River, near Bancroft, Ontario, Canada. The sample is a constituent of a nepheline – scapolite – albite – biotite gneiss. The structure of this nepheline was refined by Foreman & Peacor (1970), and Prof. Peacor has kindly provided this sample for our study. McConnell (1962) noted that specimens from this locality exhibit relatively sharp satellite reflections. Nepheline crystals were hand-picked under a binocular microscope, and the crystals were finely ground in an

agate mortar and pestle for powder X-ray diffraction (XRD), transmission electron microscopy (TEM), and thermal analyses. A single-crystal fragment was selected for structure refinement using a Bruker P4 automated four-circle single-crystal X-ray diffractometer and graphite-monochromatized  $\text{MoK}\alpha$  radiation. The  $\theta$  –  $2\theta$  scan mode was used to collect the data using variable scan rates. The structure refinement was done using the *Shelxtl97* suite of programs (Sheldrick 1997).

A Siemens D5000 X-ray powder diffractometer, operating in a vertical position and in the  $\theta$ – $\theta$  geometry, was used to obtain a XRD trace in the  $2\theta$  range of 10 to  $80^\circ$ . Using  $\text{CuK}\alpha$  radiation in conjunction with a position-sensitive detector, data were collected in a continuous scan with a step size of  $0.015^\circ$  and step time of 15.0 s. Data were collected from 25 to  $1300^\circ\text{C}$ . The room-temperature cell parameters were determined by least-squares refinement using the Siemens program

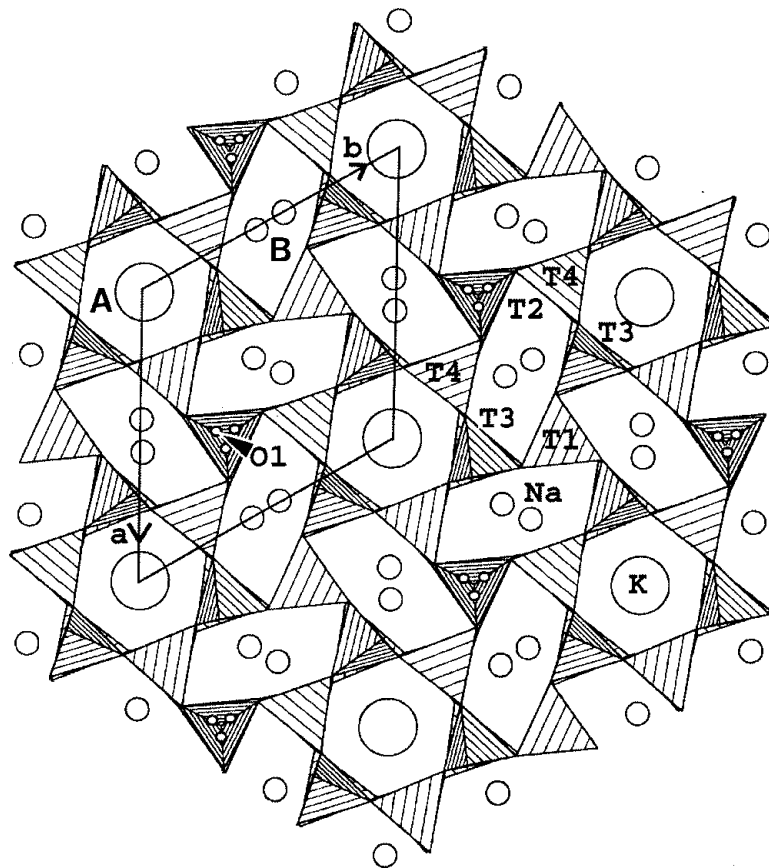


FIG. 1. Crystal structure of nepheline projected down the  $c$  axis. A is the hexagonal site that contains K and vacancies, and B is the oval site containing Na and Ca. The  $T_2$  and  $T_3$  tetrahedra have apices pointing upward, and  $T_1$  and  $T_4$  point downward. The O1 atom is disordered over three positions in the average structure.

WIN-METRIC. The cell parameters (hexagonal cell) at 25°C are  $a$  9.9934(9),  $c$  8.3769(9) Å. These parameters agree with those obtained by Foreman & Peacor (1970) and the results obtained by single-crystal XRD (see below, Tables 2 and 7). Applying the XRD method of Smith & Sahama (1954) and using the cell parameters given above, the deduced composition agrees with those of Tilley (1954) and Foreman & Peacor (1970) for specimens from the same locality.

Crystal fragments were placed on holey-carbon support copper grids, and TEM data were recorded from thin regions of the crystal fragments. Electron microscopy was performed using a JEOL JEM-3010 transmission electron microscope operating at 300 keV with a LaB<sub>6</sub> filament and equipped with a ±20° double-tilt, side-entry goniometer holder. An ultra-high-resolution pole piece ( $C_s = 0.6$  mm) was used, and the point-to-point resolution was better than 1.7 Å. Scherzer focus is -415 Å from the Gaussian focus, where minimum contrast occurs. Images were observed with a Gatan TV camera and an image intensifier. TEM images were recorded using the minimum exposure mode.

Thermal analyses were carried out with a computerized, Shimadzu Thermal System 50 (TG 50, DTA 50, and DSC 50) using similar Al<sub>2</sub>O<sub>3</sub> crucibles for the sample and an empty crucible for the reference. A furnace was placed over the sample and reference crucibles, and both were heated in a controlled manner using a microprocessor-controlled programmer. For the thermogravimetric (TG) experiment, 9.1 mg of powdered nepheline was heated at a rate of 10°C/min. from room temperature to 1000°C in a dynamic air atmosphere where the flow rate of air was 60 mL/min. For the differential thermal analysis (DTA), 17.4 mg of powder sample was heated using the same parameters as were used for the TG experiment. For the differential scanning calorimetry (DSC) experiment, 6.0 mg of a powder sample was heated at a rate of 10°C/min from room temperature to 500°C in a dynamic nitrogen atmosphere, where the flow rate of nitrogen was 60 mL/min. The thermal data were analyzed using Shimadzu software programs provided with the instruments. The

TG curve was corrected for buoyancy effect, and the DTA curve was corrected for baseline effect. The relationship between change in enthalpy and peak area in the DTA and DSC curves was determined by calibration using different standard materials. The area under the peak in the DSC curve is the integrated total energy involved in the reaction, whereas the displacement of the baseline provides the specific heat of the sample. DSC is more sensitive than DTA and less likely to be affected by changes in operational variables, such as heating rate, fineness of grain size, etc.

The nepheline sample was also run to 1150°C at a heating rate of 10°C/min. in a static air environment using a Netzsch STA simultaneous TG-DSC equipment. Two runs were made, with different amount of samples (6.5 and 13.6 mg, respectively).

A chemical analysis was done using a Cameca Camebax electron microprobe (EMP) using the operating program MBX (copyright held by Carl Henderson, University of Michigan), and the correction was done using Cameca's PAP program. The analytical conditions were 15 kV and 9.5 nA beam current. Natural minerals were used as standards: for example, microcline (SiK $\alpha$ , KK $\alpha$ ), albite (NaK $\alpha$ ), anorthite (AlK $\alpha$ , CaK $\alpha$ ), and apatite (PK $\alpha$ ). The oxide weight percentages resulting from the EMP analyses are given (Table 1). A diffuse beam of electrons was used for the analysis to avoid the loss of Na and K. The chemical formula obtained for nepheline is comparable to that in the literature (see below, Table 7).

#### STRUCTURE REFINEMENT OF NEPHELINE

Unit-cell parameters were obtained by least-squares refinement using 42 reflections with  $2\theta$  between 10 and 26° and automatically aligned on a single-crystal diffractometer. The cell parameters and other information regarding data collection and refinement are given in Table 2.

The single-crystal data were corrected for Lorentz, polarization, background effects, and empirical absorption (Table 2). Initial structural parameters were those obtained by Foreman & Peacor (1970). The refinement was carried out in the sequence of refining scale, atom positions, isotropic, and then anisotropic displacement parameters. Finally, all variables were refined simultaneously. In the final stages of the refinement, the site-occupancy factors (*sof*) of Na, K, Al, and Si were adjusted slightly from those given in the chemical formula, and the final formula obtained by refinement is that given in Table 2. The final  $R_1$  index is 0.041.

The positional coordinates and equivalent isotropic displacement parameters are given in Table 3, and anisotropic displacement parameters are listed in Table 4. The bond distances and angles are given in Tables 5 and 6, respectively, and important distances are compared to other datasets in Table 7. Tables of observed and calculated structure-factors are available from the Depository

TABLE 1. CHEMICAL COMPOSITION FOR NEPHELINE FROM EGAN CHUTE, BANCROFT AREA, ONTARIO

SiO <sub>2</sub> wt.%	42.68	Si <i>apfu</i>	8.21
Al <sub>2</sub> O <sub>3</sub>	34.25	Al	7.77
Na <sub>2</sub> O	16.23	$\Sigma$	15.98
K <sub>2</sub> O	5.38	Na	6.05
CaO	1.09	K	1.32
MnO	0.01	Ca	0.22
P <sub>2</sub> O <sub>5</sub>	0.02	$\Sigma$	7.59
Others	0.04	Mn	0.00
$\Sigma$	99.67	P	0.00

The formula (K<sub>1.32</sub>□<sub>0.68</sub>X(Na<sub>6.05</sub>Ca<sub>0.22</sub>)Al<sub>7.77</sub>Si<sub>8.21</sub>O<sub>32</sub>) was obtained from the analytical data on the basis of 32 oxygen atoms per formula unit (*apfu*).

of Unpublished Data, CISTI, National Research Council, Ottawa, Ontario K1A 0S2, Canada.

The general features of the structure of nepheline have been described above, and topologically our refined structure corresponds to that established in other refinements. All the atom positions and temperature factors for our nepheline sample are normal and similar to those from other well-refined framework silicates. Except for the O1 oxygen atom, which is displaced slightly from the threefold axis, the atoms do not indicate positional disorder. The Al–O and Si–O distances indicate that the Al and Si atoms are fully ordered (Table 5). This ordering is further justified by bond-strength calculations (Wills & Brown 1999). The bond-strength sums for the O atoms are close to the expected value of 2 valence units (*v.u.*; Table 5). However, the

bond-strength sum for the O1 atom indicates that it is underbonded, which reflect the fact that the O1 position is not well defined. The bond-strength sums for Al1, Al4, and Si3 are very close to the expected values of 3 *v.u.* for Al<sup>3+</sup> and 4 *v.u.* for Si<sup>4+</sup>, but the value for Si2 indicates a slight excess charge (Table 5). The excess charge on Si2 may arise from the fact that the O1 position is not well defined. Excess Si over Al was not detected by the refinement. The refinement confirms that the K site contains vacancies, and that the Na site is fully occupied by Na atoms. The presence of Ca, which typically substitutes for Na, was not directly detected in the structure refinement. The refinement indicates that the

TABLE 2. CRYSTAL AND STRUCTURE-REFINEMENT DATA FOR NEPHELINE FROM EGAN CHUTE

Empirical formula	$K_{1.35}Ca_{0.65}Na_6[Al_3Si_6O_{32}]$
Formula weight	1143.29
Temperature	297(2) K
$\lambda_{MoK\alpha}$	0.71073 Å
Crystal system, space group	Hexagonal; $P6_3$
Unit-cell dimensions	$a = b = 9.9853(7)$ , $c = 8.3689(17)$ Å
Volume	$V = 722.64(16)$ Å <sup>3</sup>
$Z$ , $D_{calc}$	1; 2.627 Mg/m <sup>3</sup>
Absorption coefficients	$\mu = 1.033$ mm <sup>-1</sup> ; $\mu_r = 0.16$
$F(000)$	564
Crystal size	0.15 × 0.15 × 0.15 mm
$\theta$ range for data collection	2.36 to 32.48°
Limiting indices	$-1 \leq h \leq 13$ , $-15 \leq k \leq 1$ , $-1 \leq l \leq 2$
Reflections collected / unique	2415 / 1024; [R(int) = 0.0428]
Completeness to $\theta = 32.48$	99.8%
Absorption correction	Empirical
Max. and min. transmission	0.90 and 0.71
Refinement method	Full-matrix least-squares on $F^2$
Data / restraints / parameters	1024 / 1 / 91
Goodness-of-fit on $F^2$	1.081
Final R [ $I > 2\sigma(I) = 737$ obs. reflections]	$R_1 = 0.0410$ , $wR_2 = 0.0898$
R indices (all data = 1024 reflections)	$R_1 = 0.0638$ , $wR_2 = 0.1079$
Absolute structure parameter	-0.3(5)
Largest diff. peak and hole	0.699 and -0.574 e/Å <sup>3</sup>

TABLE 3. ATOM COORDINATES AND EQUIVALENT ISOTROPIC DISPLACEMENT PARAMETERS (Å<sup>2</sup>) FOR NEPHELINE FROM EGAN CHUTE, BANCROFT AREA, ONTARIO

Atoms	site	sof	x	y	z	$U_{eq}^*$
Al1	2b	0.33	0.6667	0.3333	0.1907(6)	0.011(1)
Si2	2b	0.33	0.6667	0.3333	0.8024(6)	0.013(1)
Si3	6c	1.0	0.3339(3)	0.0939(2)	0.3103(2)	0.012(1)
Al4	6c	1.0	0.3321(3)	0.0931(3)	0.6838(2)	0.011(1)
K1	2a	0.675	0	0	0.9920(14)	0.026(1)
Na1	6c	1.0	0.4429(2)	0.9970(2)	0.9952(10)	0.023(1)
O1	6c	0.33	0.7113(11)	0.3470(60)	0.9850(20)	0.030(5)
O2	6c	1.0	0.3174(5)	0.0272(4)	0.4911(13)	0.029(1)
O3	6c	1.0	0.5238(6)	0.1731(7)	0.7348(17)	0.034(2)
O4	6c	1.0	0.5095(7)	0.1621(7)	0.2487(16)	0.031(2)
O5	6c	1.0	0.2857(7)	0.2271(8)	0.3113(14)	0.020(1)
O6	6c	1.0	0.2679(7)	0.2239(8)	0.6881(14)	0.022(1)

\*  $U_{eq}$  is defined as one third of the trace of the orthogonalized  $U_{ij}$  tensor.

TABLE 4. ANISOTROPIC DISPLACEMENT PARAMETERS (Å<sup>2</sup>) FOR NEPHELINE FROM EGAN CHUTE, BANCROFT AREA, ONTARIO

Atoms	$U_{11}$	$U_{22}$	$U_{33}$	$U_{23}$	$U_{13}$	$U_{12}$
Al1	0.012(1)	0.012(1)	0.010(2)	0	0	0.006(1)
Si2	0.013(1)	0.013(1)	0.012(2)	0	0	0.007(1)
Si3	0.013(1)	0.010(1)	0.014(1)	0.000(1)	0.000(1)	0.005(1)
Al4	0.011(1)	0.009(1)	0.013(1)	0.000(1)	0.001(1)	0.005(1)
K1	0.022(1)	0.022(1)	0.034(2)	0	0	0.011(1)
Na1	0.020(1)	0.029(1)	0.018(1)	0.001(3)	-0.002(2)	0.012(1)
O1	0.029(6)	0.046(7)	0.003(5)	-0.007(14)	0.006(6)	0.008(13)
O2	0.056(2)	0.028(2)	0.014(2)	0.001(4)	0.001(4)	0.029(2)
O3	0.012(2)	0.012(2)	0.075(6)	-0.001(3)	-0.005(3)	0.005(2)
O4	0.011(2)	0.013(2)	0.066(5)	0.002(3)	0.005(3)	0.004(2)
O5	0.025(2)	0.018(2)	0.018(3)	0.005(3)	0.004(3)	0.013(2)
O6	0.029(3)	0.018(3)	0.023(3)	-0.003(3)	-0.002(3)	0.016(2)

The anisotropic displacement factor exponent takes the form:  $-2\pi^2[h^2a^{*2}U_{11} + \dots + 2hka^*b^*U_{12}]$

TABLE 5. BOND DISTANCES [Å] AND BOND STRENGTHS<sup>†</sup> (*v.u.*) FOR NEPHELINE FROM EGAN CHUTE

Al1	-O1	1.77(2) Å	0.667 <i>v.u.</i>	Na1	-O1	2.566(11) Å	0.129 <i>v.u.</i>
	-O4: ×3	1.714(6)	0.776 ×3		-O2	2.523(4)	0.143
<b>Ave.</b>		<b>1.728</b>	<b><math>\Sigma = 2.995</math></b>		-O3	2.659(15)	0.099
					-O3	2.753(13)	0.077
Al4	-O2	1.721(11)	0.757		-O4	2.563(15)	0.129
	-O3	1.719(7)	0.765		-O4	2.785(14)	0.071
	-O5	1.715(9)	0.771		-O5	2.475(10)	0.163
	-O6	1.719(6)	0.767		-O6	2.581(10)	0.123
<b>Ave.</b>		<b>1.719</b>	<b><math>\Sigma = 3.060</math></b>	<b>Ave.</b>	<b>2.613</b>	<b><math>\Sigma = 0.934</math></b>	
Si2	-O1	1.58(2)	1.126	K1	-O2: ×3	3.042(4)	0.085 ×3
	-O3: ×3	1.623(7)	1.003 ×3		-O5: ×3	3.016(9)	0.091 ×3
<b>Ave.</b>		<b>1.612</b>	<b><math>\Sigma = 4.135</math></b>		-O6: ×3	2.978(11)	0.101 ×3
				<b>Ave.</b>	<b>3.015</b>	<b><math>\Sigma = 0.831</math></b>	
Si3	-O2	1.628(11)	0.989		O1	-O1	0.69(2)
	-O4	1.615(7)	1.019				
	-O5	1.626(6)	0.996				
	-O6	1.624(9)	0.998				
<b>Ave.</b>		<b>1.623</b>	<b><math>\Sigma = 4.002</math></b>				

<sup>†</sup> Bond-strengths sums for O atoms (expected value is 2.0 *v.u.*):

O1:  $\Sigma = 0.667 + 1.126 + 0.129 = 1.922$  *v.u.*  
 O2:  $\Sigma = 0.757 + 0.989 + 0.143 + 0.085 = 1.974$  *v.u.*  
 O3:  $\Sigma = 0.765 + 1.003 + 0.099 + 0.077 = 1.944$  *v.u.*  
 O4:  $\Sigma = 0.776 + 1.019 + 0.129 + 0.071 = 1.995$  *v.u.*  
 O5:  $\Sigma = 0.771 + 0.996 + 0.163 + 0.091 = 2.021$  *v.u.*  
 O6:  $\Sigma = 0.767 + 0.998 + 0.123 + 0.101 = 1.989$  *v.u.*

K site contains 1.35 K and 0.65 □ (vacancy), which agrees well with our chemical data. The bond-strength sum for the Na1 site is 0.934 *v.u.*, which indicates that the Na<sup>+</sup> cation is slightly underbonded, and may be compensated by incorporating a little Ca<sup>2+</sup> cation on the Na1 site. The most significant feature of the bond-strength calculations is the fact that the K1 site is severely underbonded (0.83 *v.u.* compared to 1 *v.u.* expected; Table 5). The K1 site, therefore, cannot be filled with K<sup>+</sup> cations, or contains Na and Ca cations, because the charge on the K1 site will not be satisfied. To satisfy the charge on the K1 site in our nepheline sample, vacancies must be present at the K1 site, as required by the

bond-strength calculations, and observed in the refinement. The 0.831 *v.u.* for the K1 site indicates a site-occupancy factor of 0.64, compared to 0.675 obtained by the refinement.

Using the present structure and bond-strength analysis, we expect that nepheline of high-temperature origin may contain more vacancies than in the present nepheline, or the K cations may move off the present K1 site to form reasonable bonds with the framework oxygen atoms. In the latter case, Na and Ca atoms may then be substituted for K atoms. These predictions are confirmed to a certain extent by previous refinements of the structure. The high-temperature nepheline #1 and #4 contain more vacancies than our sample #10a, b (Table 7). For nepheline #3, the Na atom is moved off the present K1 site to form reasonable bond-distances. However, for nepheline #5, it is surprising to see that the K1 site is occupied by nearly one K and one Na atom because the charge on the Na atom on the K1 site can never be satisfied, as indicated by our calculations.

#### DISCUSSION OF THE NEPHELINE STRUCTURE

The results of ten structure refinements of various natural and synthetic samples of nepheline are available (Table 7). The entries 10a and 10b in Table 7 are based on cell parameters obtained in this present study by single-crystal XRD and powder XRD, respectively. Nepheline has several unusual features, which are discussed below with the results from this study.

TABLE 6. BOND ANGLES [°] FOR NEPHELINE FROM EGAN CHUTE

O4-A11-O1	110.0(18)	O1-Si2-O3	96.1(9)
O4-A11-O1	93.8(9)	O1-Si2-O3	119.5(16)
O4-A11-O1	114.9(13)	O1-Si2-O3	114.0(2)
O4-A11-O4	112.3(4) × 3	O3-Si2-O3	108.5(5) × 3
<b>Ave.</b>	<b>109.3</b>	<b>Ave.</b>	<b>109.2</b>
O4-Si3-O2	109.6(5)	O3-A14-O2	105.9(5)
O4-Si3-O5	111.1(4)	O5-A14-O3	107.6(5)
O4-Si3-O6	106.8(5)	O5-A14-O2	110.4(4)
O5-Si3-O2	108.6(5)	O5-A14-O6	111.2(4)
O6-Si3-O2	110.5(4)	O6-A14-O2	108.5(5)
O6-Si3-O5	110.2(4)	O6-A14-O3	113.2(4)
<b>Ave.</b>	<b>109.5</b>	<b>Ave.</b>	<b>109.5</b>
Si2-O1-A11	152.5(9)	Si3-O4-A11	140.4(5)
Si3-O2-A14	138.0(2)	Si3-O5-A14	141.2(8)
Si2-O3-A14	140.4(5)	Si3-O6-A14	141.5(8)

TABLE 7. CHEMICAL COMPOSITION, UNIT-CELL PARAMETERS, AND MEAN BOND-DISTANCES (Å) FOR NEPHELINE SAMPLES OF DIFFERENT ORIGINS

Sample	A site	B site	Framework	<i>a</i>	<i>c</i>	A-O	Na-O	<i>T</i> <sub>1</sub>	<i>T</i> <sub>2</sub>	<i>T</i> <sub>3</sub>	<i>T</i> <sub>4</sub>	<i>T</i> <sub>1</sub> - <i>T</i> <sub>4</sub>	<i>T</i> <sub>2</sub> - <i>T</i> <sub>3</sub>	<i>R</i>
1	[K <sub>1.28</sub> □ <sub>0.72</sub> ] <sub>Σ2.0</sub>	[Na <sub>5.36</sub> Ca <sub>0.28</sub> ] <sub>Σ5.64</sub>	[Al <sub>7.92</sub> Si <sub>8.08</sub> ] <sub>Σ16.0</sub> O <sub>32</sub>	10.003	8.381	3.017	2.630	1.697	1.651	1.628	1.718	-0.021	0.023	0.062
2	[K <sub>1.40</sub> □ <sub>0.60</sub> ] <sub>Σ2.0</sub>	[Na <sub>5.50</sub> Ca <sub>0.30</sub> ] <sub>Σ5.80</sub>	[Al <sub>7.50</sub> Si <sub>8.50</sub> ] <sub>Σ16.0</sub> O <sub>32</sub>	10.007	8.385	3.024	2.622	1.693	1.649	1.624	1.725	-0.032	0.025	0.080
3	[Na <sub>1.50</sub> □ <sub>0.50</sub> ] <sub>Σ2.0</sub>	[Na <sub>5.80</sub> Ca <sub>0.20</sub> ] <sub>Σ6.00</sub>	[Al <sub>7.50</sub> Si <sub>8.50</sub> ] <sub>Σ16.0</sub> O <sub>32</sub>	9.968	8.356	2.984	2.619	1.680	1.650	1.625	1.714	-0.034	0.025	0.074
4	[K <sub>0.24</sub> □ <sub>1.76</sub> ] <sub>Σ2.0</sub>	Na <sub>6</sub>	[Al <sub>6.24</sub> Si <sub>9.76</sub> ] <sub>Σ16.0</sub> O <sub>32</sub>	9.964	8.360	3.026	2.611	1.629	1.691	1.664	1.667	-0.038	0.027	0.063
5	[K <sub>0.96</sub> Na <sub>0.96</sub> □ <sub>0.08</sub> ] <sub>Σ2.0</sub>	Na <sub>6</sub>	[Al <sub>7.92</sub> Si <sub>8.08</sub> ] <sub>Σ16.0</sub> O <sub>32</sub>	9.989	8.380	2.987	2.629	1.730	1.624	1.621	1.726	0.004	0.003	0.064
6	[K <sub>1.32</sub> □ <sub>0.68</sub> ] <sub>Σ2.0</sub>	[Na <sub>5.64</sub> Ca <sub>0.36</sub> ] <sub>Σ6.00</sub>	[Al <sub>7.92</sub> Si <sub>8.08</sub> ] <sub>Σ16.0</sub> O <sub>32</sub>	9.993	8.374	3.007	2.622	1.725	1.642	1.623	1.744	-0.019	0.019	0.053
7	[K <sub>1.01</sub> □ <sub>0.99</sub> ] <sub>Σ2.0</sub>	Na <sub>6.04</sub>	[Al <sub>7.72</sub> Si <sub>8.15</sub> ] <sub>Σ15.87</sub> O <sub>32</sub>	9.9995	8.384	2.999	2.633	1.731	1.606	1.616	1.736	-0.005	-0.010	0.018
8	[K <sub>1.60</sub> □ <sub>0.40</sub> ] <sub>Σ2.0</sub>	[Na <sub>6.21</sub> Ca <sub>0.06</sub> ] <sub>Σ6.27</sub>	[Al <sub>7.43</sub> Si <sub>8.44</sub> ] <sub>Σ15.87</sub> O <sub>32</sub>	9.985	8.372	3.009	2.632	1.723	1.603	1.615	1.728	-0.005	-0.012	0.027
9	[K <sub>1.76</sub> □ <sub>0.24</sub> ] <sub>Σ2.0</sub>	[Na <sub>5.86</sub> Ca <sub>0.13</sub> ] <sub>Σ5.99</sub>	[Al <sub>7.84</sub> Si <sub>8.12</sub> ] <sub>Σ15.96</sub> O <sub>32</sub>	9.9979	8.3852	3.008	2.627	1.732	1.605	1.616	1.734	-0.002	-0.011	0.017
10a	[K <sub>1.32</sub> □ <sub>0.68</sub> ] <sub>Σ2.0</sub>	[Na <sub>6.06</sub> Ca <sub>0.22</sub> ] <sub>Σ6.28</sub>	[Al <sub>7.78</sub> Si <sub>8.22</sub> ] <sub>Σ16.0</sub> O <sub>32</sub>	9.9853	8.3689	3.015	2.613	1.728	1.612	1.623	1.719	0.007	-0.011	0.041
10b	[K <sub>1.32</sub> □ <sub>0.68</sub> ] <sub>Σ2.0</sub>	[Na <sub>6.06</sub> Ca <sub>0.22</sub> ] <sub>Σ6.28</sub>	[Al <sub>7.78</sub> Si <sub>8.22</sub> ] <sub>Σ16.0</sub> O <sub>32</sub>	9.9934	8.3769	3.015	2.616	1.730	1.613	1.625	1.720	0.010	-0.012	0.041
<b>Ave.</b>				<b>9.9896</b>	<b>8.3748</b>	<b>3.008</b>	<b>2.623</b>	<b>1.709</b>	<b>1.631</b>	<b>1.625</b>	<b>1.721</b>	<b>-0.012</b>	<b>0.006</b>	

1. Monte Somma, Italy (Simmons & Peacor 1972). 2. Larvik, Norway (Dollase 1970). 3. Na-exchanged Larvik nepheline (Dollase & Peacor 1971, Dollase & Thomas 1978). 4. Hydrothermally synthesized (Dollase & Thomas 1978). 5. Synthesized from NaF (Gregorkiewicz 1984). 6. Bancroft, Ontario (Foreman & Peacor 1970). 7. Khibina-Lovozero complex, Kola Peninsula, Russia (Tait *et al.* 2003). 8. Bancroft, Ontario, Canada (Tait *et al.* 2003). 9. Monte Somma, Italy (Tait *et al.* 2003). 10a. Egan Chute, Bancroft, Ontario (this study, based on single-crystal XRD cell parameters). 10b. This study, based on powder XRD cell parameters. *T*<sub>1</sub> and *T*<sub>4</sub> are Al-rich; *T*<sub>2</sub> and *T*<sub>3</sub> are Si-rich (see text).

Chemical analyses of natural nepheline indicate an excess of Si relative to Al (Fig. 2). Results of seventy-seven (77) chemical analyses of nepheline specimens of different geological origins were taken from the literature (Bannister & Hey 1931, Smith & Sahama 1954, Dollase & Peacor 1971, Dollase & Thomas 1978, Ikovskiy 1980). These chemical data were recalculated on the basis of 32 oxygen atoms. The chemical analyses indicate that all nepheline specimens deviate from the ideal composition  $(K,Na)_8Al_8Si_8O_{32}$ , for  $Z = 1$ , with the following average value (in atoms per formula unit, *apfu*): Si = 8.38, Al = 7.48, Na = 5.80, K = 1.56, Ca = 0.16, vacancy,  $\square = 0.40$ , and Mg + Fe + Mn + Ti = 0.13. Although the sum of Si and Al atoms is close to the ideal unit-cell content of 16, the nepheline samples contain more Si than Al atoms (Fig. 2). If the excess Si over Al atoms (*i.e.*, Si minus Al) is plotted against the number of vacancies (diagram not shown), the "excess" of Si atoms is accompanied by an increase in the number of vacancies at the A sites, as indicated by  $\square$  in the general formula,  $Na_xK_yCa_z\square_{8-(x+y+z)}Al_{(x+y+2z)}Si_{16-(x+y+2z)}O_{32}$  (see Deer *et al.* 1992). Further vacancies arise from substitution of Ca for Na atoms. Structure refinements have failed to directly locate this excess Si. In our refinement, no Ca atom was detected, but the presence of Ca was implied by bond-strength calculations and the chemical analysis. The amount of vacancies found at the K site is 0.65, which requires the following theoretical charge-balance formula:  $(K_{1.35}\square_{0.65})Na_6[Al_{7.35}Si_{8.65}O_{32}]$ . However, the deduced chemical composition based on cell parameters gave the formula,

$(K_{1.35}\square_{0.65})(Na_6Ca_{0.36})[Al_{7.93}Si_{8.07}O_{32}]$ , and the formula obtained by EMP analysis is  $(K_{1.32}\square_{0.68})(Na_{6.05}Ca_{0.22})[Al_{7.77}Si_{8.21}O_{32}]$ , but in our structure refinement, the formula  $(K_{1.35}\square_{0.65})Na_6[Al_8Si_8O_{32}]$  was obtained. The latter formula is justified by bond-strength calculations.

The K atom is coordinated by nine O atoms, and the Na atom is coordinated by either seven or eight O atoms (Dollase 1970). In our specimen, the Na atom is coordinated by eight O atoms. From the chemical compositions and structures, Na and Ca atoms fully occupy the six B cavities, so the average Na–O bond is expected to be nearly constant, or vary within a narrow range (Table 7). In terms of the Na–O distances, there are no significant differences among the samples because the Na1 site is nearly fully occupied by Na atoms, with only a minor amount of Ca atoms. The K atoms occupy nearly two-thirds of the A cavities in natural samples and are replaced to various extents by vacancies or Na in synthetic nepheline, but the average A–O distance varies within a narrow range (Table 7). Our bond-strength calculations indicate that Na atoms cannot substitute for K atoms and still be charge-satisfied. The K site cannot be fully occupied and still be charge-balanced, as indicated by the bond-strength calculations. However, Tait *et al.* (2003) examined a sample of nepheline in which the A site is nearly fully occupied by K atoms (sample #7), but their bond-strength calculations show this site to be underbonded. For the Na-exchanged Larvik nepheline, the Na atoms in the A site were statistically distributed closer to some of the O atoms on the wall of the cavity to obtain nearly normal

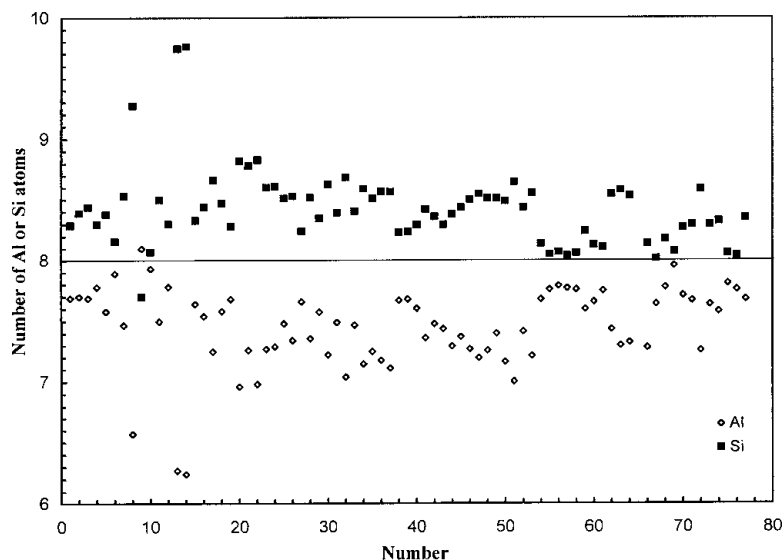


FIG. 2. Variation in proportion of Al and Si atoms in 77 specimens of nepheline, indicating that Si > Al.

Na–O bonds (Table 7, sample #3; Dollase & Peacor 1971, Dollase & Thomas 1978). Therefore, it is surprising to observe that in the Na-rich synthetic nepheline, both the Na and K atoms occur at the K1 site (Table 7, sample #5; Gregorkiewitz 1984). The A–O distances show that those samples with significant Na atoms at the K1 site have the shortest A–O distances (samples #3 and #5). Those samples of nepheline with the highest vacancies at the K1 site have the longest A–O distances (sample #4). Those samples with similar number of vacancies have similar A–O distances (Table 7). Therefore, the A cavities are able to adapt to the different occupancies at the site.

Al and Si are ordered over the tetrahedral sites in nepheline. In general, the  $T_1$  and  $T_4$  sites are Al-rich, and the  $T_2$  and  $T_3$  sites are Si-rich (Table 7). Al–Si disorder increases with temperature in the sequence: gneissic – plutonic – volcanic (Dollase & Peacor 1971). However, Tait *et al.* (2003) have suggested that in nepheline of whatever origin, the degree of Al–Si order is high. NMR spectroscopic data indicate high degrees of order in natural and synthetic samples of nepheline (Lippmaa *et al.* 1980, Stebbins *et al.* 1986, Hovis *et al.* 1992). The  $T$ –O distances for all previous structure refinements (Table 7), when used to calculate tetrahedral site occupancies, gave values of total Al and Si that are inconsistent with totals derived from chemical analyses. The number of Si atoms derived from  $T$ –O distances is as high as 8.9 compared to a maximum of 8.5 from chemical analyses (*e.g.*, Dollase & Peacor 1971, Simmons & Peacor 1972). Because  $T_1$  and  $T_2$  are those tetrahedra whose O1 atom is disordered, Gregorkiewitz (1984) attributed a tilting of  $T_1$  and  $T_2$  tetrahedra to a release of strain and the attainment of a proper Na–O1 bond distance. Consequently, the atoms O3 and O4 must shift in response to the displacement of O1 because of the rigidity of  $TO_4$  tetrahedra. This shift is indicated by large anisotropic thermal motion of these atoms, with the largest vibrations along the  $c$  axis and sharp maxima in the difference synthesis (Dollase 1970, Gregorkiewitz 1984). The observed distances in  $T_1$  and  $T_2$  tetrahedra reflect the tilting of tetrahedra more than the Al–Si distribution (Gregorkiewitz 1984). In our structure refinement, we do not observe such unusual features, and we obtain  $T$ –O distances that indicate a fully ordered Al–Si distribution (Fig. 3a; sample #10a, b).

Another test for Al and Si ordering may be made by analyzing the differences in order on the  $T_1$  and  $T_4$  sites on the one hand, and the  $T_2$  and  $T_3$  sites on the other. If only Al occupies the  $T_1$  and  $T_4$  sites, the difference between average  $\langle T_1$ –O  $\rangle$  and  $\langle T_4$ –O  $\rangle$ , denoted  $T_1$ – $T_4$ , should be small (Table 7, Fig. 3a). Similarly, if Si occupies the  $T_2$  and  $T_3$  sites, then  $T_2$ – $T_3$ , must be small. The data tend to cluster into two groups: group 1 contains samples #5, #7–9, and #10a, b, where the degree of Al–Si order is high. Sample #6 should be included with group 1, but is excluded because the  $\langle T_2$ –O  $\rangle$  value is too high (Table 7), and we have obtained better values

for this sample in the present study. Group 2 contains samples #4, #3, #2, and #1, where the degree of Al–Si order is not high.

The isotropic displacement parameters for previously refined structures are exceptionally large, about three times those values obtained for well-ordered silicate structures. These large displacement parameters may result from positional disorder averaged over domains (*e.g.*, Simmons & Peacor 1972). However, in this study, we obtained reasonable displacement-parameters for all the atoms in nepheline (Table 3).

The O1 oxygen atom is displaced from the three-fold axis in all refined structures, and occupies one of these three positions in different unit-cells (Table 3). This displacement results from the adjustment of the O1 position to form reasonable Na–O1 bonds and satisfies the

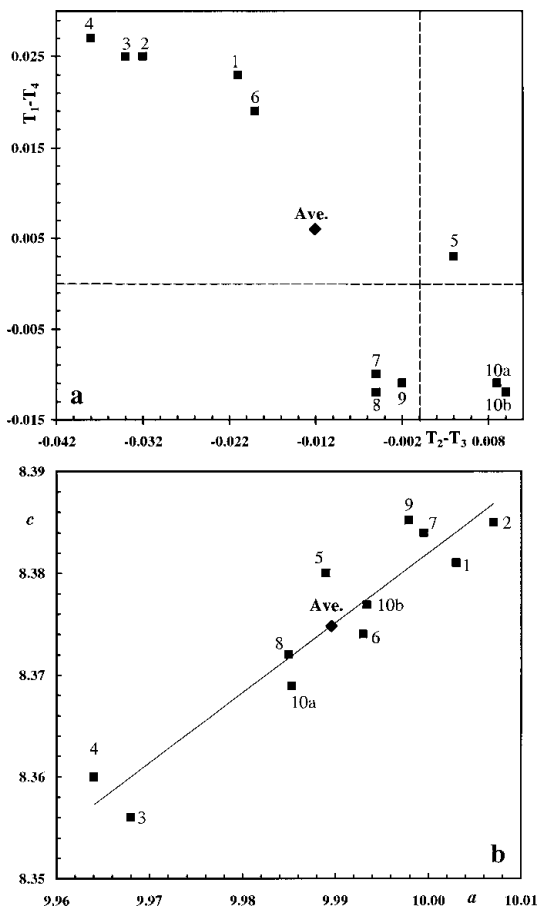


FIG. 3. (a) Difference between average  $\langle T_1 - T_4 \rangle$  versus  $\langle T_2 - T_3 \rangle$  distances showing the existence of ordered and disordered nephelines. (b) Cell parameter  $c$  versus  $a$  showing an apparent linear relationship in nepheline (Table 7).

local charge-balance (Dollase 1970). The O1 position gives rise to unusual distorted geometry for the Al1 and Si2 tetrahedra in all refined structures. For example, the O4 – Al1 – O1 angle is 94° and the O3 – Si2 – O1 angle is 120° (Table 6). The disorder of O1, resulting unusual angles, rigidity of the TO<sub>4</sub> group, and large displacement-parameters indicate that the other atoms in nepheline, O4 and O3, for example, must shift, so these atoms probably represent average positions (*e.g.*, Simmons & Peacor 1972, Gregorkiewitz 1984). In our structure, except for O1 disorder, no other unusual features were observed. Therefore, we suggest that the refined O1 position is still an average position and in individual cells; it will shift from its present position to produce reasonable angles and bond lengths.

Tait *et al.* (2003) have examined the crystal structures of three samples; crystal-structure results were reported from two of these localities, and the Al–Si order documented was in contrast with previous work. Bond distances depend on cell parameters. There is an apparent linear relationship between the cell parameters in nepheline (Fig. 3b, Table 7). Samples #3 and #4 have the smallest unit-cell parameters, and they have a lower degree of order of Al and Si than the average values (Fig. 3a). Both cell parameters for samples #1 and #2 are within the normal range, but the degree of Al–Si order is not high (Fig. 3). Therefore, differences in cell parameters cannot account for the range of Al–Si order in all samples of nepheline.

Nepheline contains weak and diffuse satellite reflections with irrational indices (*e.g.*, McConnell 1962,

Sahama 1958). These satellite reflections may indicate the presence of a domain structure. The domain structure may result from ordering of K and vacancies at the K site (*e.g.*, Foreman & Peacor 1970), or ordering of the Al and Si atoms (*e.g.*, McConnell 1962). Structure refinements, including the present one, have failed to provide direct conclusive evidence as to the nature of the domain structure. The order of Al and Si cannot account for the formation of the supercell in nepheline.

From a study of the intensities of the satellite reflections, Parker & McConnell (1971) suggested that the supercell is the result of a coordinated displacive transformation, similar to that found in tridymite, rather than to substitutional ordering. However, from available chemical compositions and structural analyses of natural nepheline, approximately 1/3 of the two A sites are normally vacant. The A sites, therefore, contain ideally 1.33 K and 0.67 □. Tripling of the cell in the superstructure makes possible the ordering of K and □. Similarly, in the average structure, O1 occupies three equivalent sites with equal probability. Tripling the cell volume enables the O1 atom to order over the three sites throughout the structure (McConnell 1962, Foreman & Peacor 1970). If such a triple supercell exists, then it should be observable by diffraction (XRD and TEM), but no such cell was observed in this study.

#### THERMAL ANALYSES OF NEPHELINE

On heating nepheline to 1000°C, the TG analysis shows no significant loss in weight, as expected (curve not shown). The thermal curves shows four main peaks (Fig. 4). The DTA curve shows a peak at about 963°C (Table 8, Fig. 4a). This peak 4 indicates an Al–Si order–disorder transition because the transition from nepheline to “carnegieite” occurs at a higher temperature, as indicated by the phase diagram involving nepheline (Deer *et al.* 1992) and our high-temperature XRD traces show peaks that are characteristic of nepheline at this temperature and above. The DSC and DDSC curves show three well-defined peaks at relatively low temperatures (Fig. 4b, Table 8). Peak 1 at 107°C represents the loss of water vapour from the sample chamber as well as water absorbed on the sample surface, as was confirmed in a second DSC run. In the second DSC run, the sample chamber was heated up to about 150°C and then cooled to room temperature and a new batch of sample was run again, and peak 1 was not observed. Peak 1 thus arises from water vapor in the sample chamber. Peak 2 at 292°C indicates a simple displacive (*i.e.*, positional disorder) transition of the framework O1 atoms in nepheline. Peak 3 at 399°C represents K – □ disorder. Peaks 1 to 3 are absent in the DTA curve, which clearly shows that DSC is more sensitive than DTA. Our high-temperature XRD studies indicate that nepheline melts after 1200°C, but before 1300°C, because the peaks in the XRD trace at 1300°C are insignificant.

TABLE 8. THERMAL ANALYSES OF NEPHELINE FROM EGAN CHUTE

Miscellaneous	DTA	DSC	DDSC	Changes
<b>Peak 1<sup>†</sup></b>				
Onset-T (°C)		101	108	Loss of H <sub>2</sub> O from air and sample surface
Peak-T (°C)	---	107	113	
End-T (°C)		113	121	
Enthalpy (J/g)		0.27		
<b>Peak 2<sup>†</sup></b>				
Onset-T (°C)		280	278	O1 disorder
Peak-T (°C)	---	292	287	
End-T (°C)		---	294	
Enthalpy (J/g)		1.39		
<b>Peak 3<sup>‡</sup></b>				
Onset-T (°C)		380	380	K – □ disorder
Peak-T (°C)	---	399	412	
End-T (°C)		417	430	
Enthalpy (J/g)		-3.43		
<b>Peak 4<sup>†</sup></b>				
Onset-T (°C)				Al–Si disorder
Peak-T (°C)	963	---	---	
End-T (°C)				

<sup>†</sup> exothermic, <sup>‡</sup> endothermic.

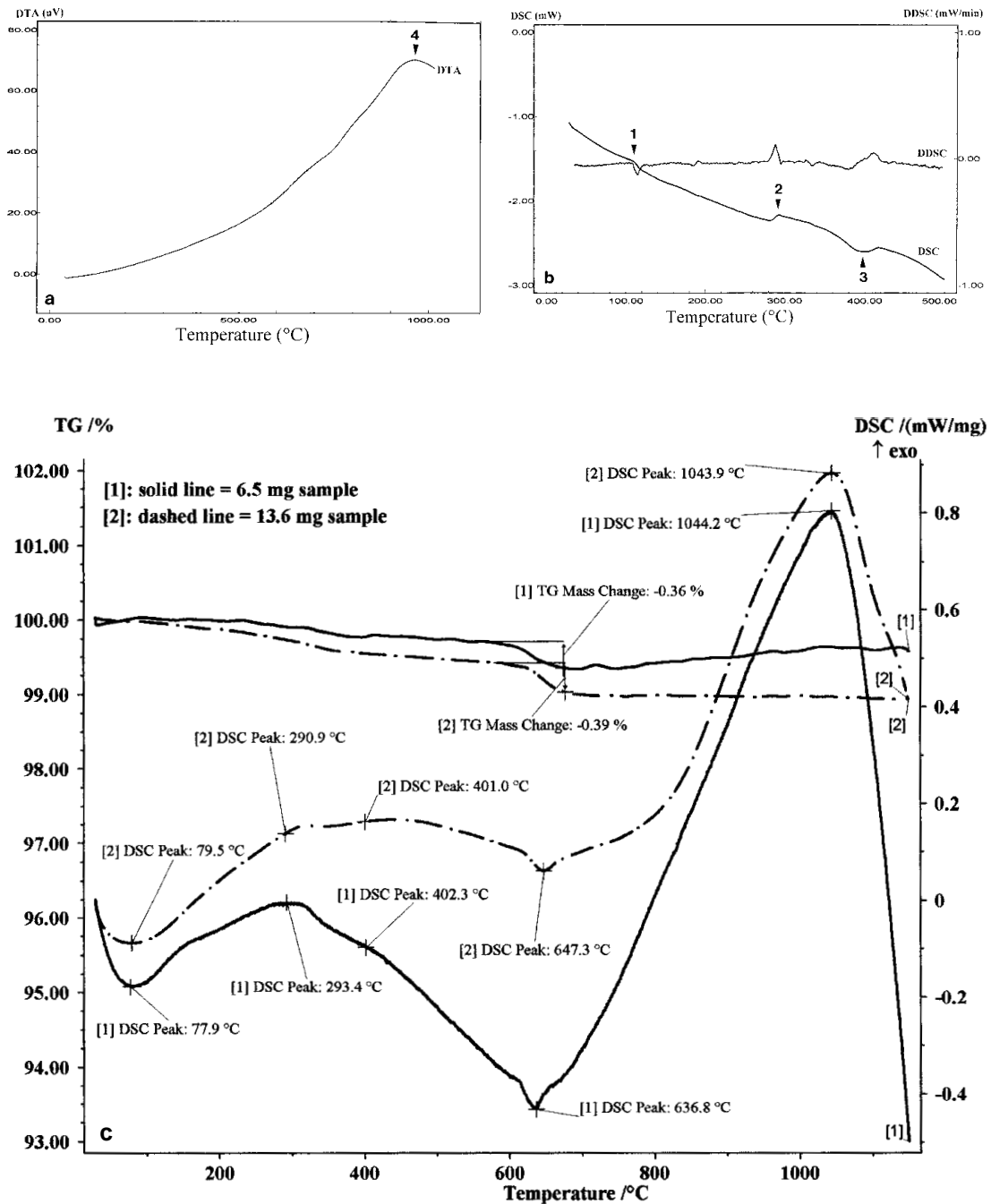


FIG. 4. Thermal curves for nepheline from Egan Chute: (a) DTA curve, (b) DSC and DDSC curves. Peaks are labeled on the DTA and DSC curves in (a) and (b), respectively. (c) TG and DSC curves showing characteristic data for nepheline.

In the second DSC run to 500°C, peak 2 occurs at 331°C and peak 3 occurs at 429°C. They are shifted by 39 and 30°C, respectively, compared to the first DSC run (Table 8). After this DSC run to 500°C, the sample was cooled to room temperature and rerun again to 500°C, but no peak was observed, which indicates that the ordering is destroyed when the sample is heated to 500°C, and the ordering is not reversible on cooling.

Because the DSC technique is more sensitive than the DTA technique, we ran the nepheline sample again to 1150°C. Two runs were made with different amounts of sample (6.5 and 13.6 mg; Fig. 4c). The TG curve shows a weight loss of 0.37% at a DSC peak temperature of about 647°C (Fig. 4c), and the DTA curve (Fig. 4a) shows a slight bulge at about the same temperature. At present, we do not know the reason for this weight loss, but it could arise from an impurity phase. Figure 4c also shows three peaks at about 292, 401 and 1044°C, and they correspond to peaks 2, 3 and 4, respectively, in Figures 4a, b. Figure 4c also shows a peak at 78°C, which is attributed to water vapor and loss of absorbed surface water. The combined thermal data show three peaks (2, 3, and 4) that occur where there is no loss in weight, so they correspond to three separate polymorphic transitions. Depending on the equipment and the sample weight, the phase transitions occur at slightly different temperatures, but in the same general range of temperature. Although all the peaks are present in TG–DSC runs using either 6.5 or 13.6 mg of samples, the peak temperatures are slightly shifted (Fig. 4c). After the DSC run to 1150°C, the cooled nepheline powder was X-rayed at room temperature; the trace indicated that the sample was still crystalline nepheline.

In a disordered nepheline, obtained by heating a sample to 750°C for several hours, Hayward *et al.* (2000) documented a displacive phase-transition to an incommensurate structure at 35°C. In a time–temperature study of the behavior of the intensity of the satellite reflections in the temperature range of 100–150°C, McConnell (1981) indicated that the experiment showed spontaneous and reversible changes in intensity of the satellite reflections on heating and cooling at low temperatures. This reversible change in intensity is attributed to a simple displacive process in the nepheline framework. Except for the temperature range, this feature may correspond to peak 2 observed in this study, and the differences in temperature may be attributed to differences in composition of the samples. The positional order–disorder transition probably involves only the framework O1 oxygen atoms, as the Al and Si atoms are fully ordered and are well defined in terms of position and displacement parameters. The other oxygen atoms in the framework are also well defined and show no unusual displacement parameters. The O1 framework atom is known to be positionally disordered and its position is not well defined, but it may be argued that the rigidity of the  $TO_4$  tetrahedra indicates that all the framework O atoms are involved in this positional

order–disorder transformation corresponding to peak 2. However, as all the framework O atoms (except O1) are well defined, it is likely that the O1 atoms mainly are involved in this transition.

McConnell (1981) indicated that irreversible changes in intensity of the satellite reflections occur at higher temperatures (greater than 150°C) and are attributed to the kinetically hindered process of disordering K ions and vacancies in the large six-fold channels of the nepheline structure. This K–□ order–disorder transformation corresponds to peak 3 at 399°C. Alkalis are certainly mobile in nepheline at this temperature.

A third order–disorder transformation corresponds to peak 4 at 963°C, which involves disorder of Al and Si. This Al–Si transition involves the highest energy, which is indicated by the area under the peak. This interpretation is consistent with the high-temperature structural results of Foreman & Peacor (1970), which show that at 900°C, the Si–O and Al–O distances are approximately equal, and our results indicate that nepheline melts at a much higher temperature.

Except for the Al–Si order–disorder process, which involves a large energy, the individual displacive and other order–disorder processes give rise to different structures with only slightly different energies (Table 8). The different structures are stable only over a restricted interval of temperature because the most favorable configuration for each of the separate O1 atoms, and the K–□ distribution is not compatible with the most favorable configuration of the other. Ordering of the O1 atoms occurs at the lowest temperature and involves the lowest energy. The ordering of the O atoms involves a simple rotation or twist of the  $TO_4$  tetrahedra and does not require much energy. The order–disorder of K–□ requires only a little more energy because the disorder occurs along the  $6_3$  channels (Table 8).

#### ELECTRON MICROSCOPY RESULTS

A SAED pattern along the [001] direction contains strong substructure reflections (Fig. 5a). A [001] HRTEM image corresponding to this SAED pattern is given (Fig. 5b). A computed fast Fourier transform (FFT) of the image is given as the upper-left insert, and it contains the main subcell reflections. The FFT was obtained by using the program *CRISP* (Hovmöller 1992). The FFT were obtained to see what reflections arise from the image, because the crystals were damaged during the TEM observations. The HRTEM image was scanned, and a square area of  $512 \times 512$  pixels was selected. A circle was selected inside the square so that the circumference of the circle was just touching the sides of the square, and a FFT was performed on the circular area, and the result was printed on a laser printer. A possible unit-cell for nepheline is indicated at the center of the image (Fig. 5b). This image should be compared with the [001] projection of the structure (Fig. 1). The edge of the unit cell is about 10 Å. The

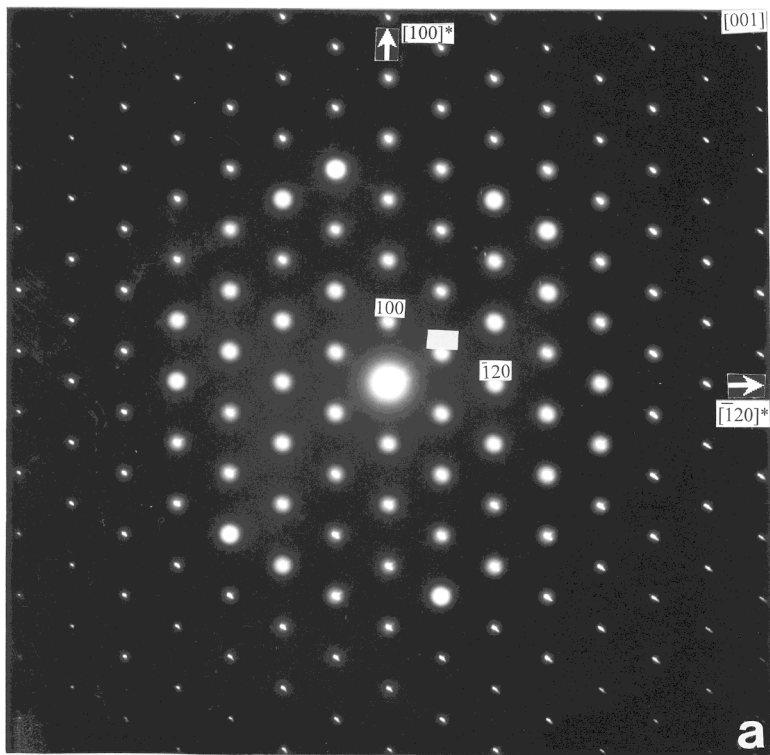


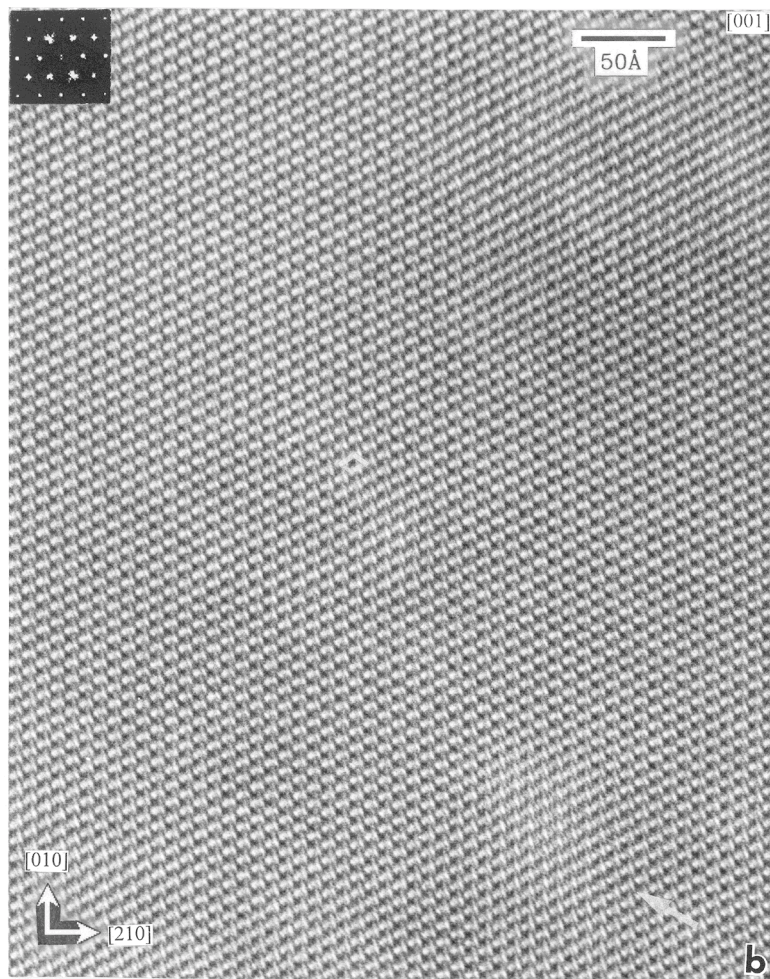
FIG. 5. a. [001] SAED pattern of nepheline from Egan Chute. b. [001] HRTEM image of nepheline from Egan Chute. A hexagonal unit-cell is outlined. Possible APBs occur at the upper- and the lower-right of the image and can be seen by viewing at a low angle along the white arrow. A FFT from the middle region of the image contains the main reflections (upper-left insert).

regular white dots at the corners of the unit cell are the hexagonal cavities, whereas the oval cavities occur in the middle and at the sides of the unit cell. This image also contains lattice fringes that are offset. The fringes are offset in two areas of the image, at upper and lower right, and are best seen by viewing at a low angle along the white arrow. These areas also have lighter contrast relative to the surrounding areas. The displacements of the fringes indicate possible out-of-phase boundaries. These may be antiphase boundaries (APBs) because the displacement of the fringes is about one-half of the repeat unit. However, the possibility that the offsets are caused by a change in crystal thickness cannot be ruled out.

The [010] SAED pattern contains strong substructure reflections and very weak satellite reflections (Fig. 6a). The satellite reflections occur at  $0.46 d_{100}$  along  $[100]^*$  and  $0.24 d_{001}$  along  $[001]^*$ . In real space, they correspond to  $18.88 \text{ \AA}$  along  $[210]$  and  $34.76 \text{ \AA}$  along  $[001]$ , respectively (Table 9). The HRTEM image corresponding to this SAED pattern and the FFT

are shown (Fig. 6b). The effect of the superstructure is not contained in this image because nepheline damages quite rapidly in the electron beam, and the satellite reflections are absent in the FFTs obtained from this image. However, the NE-running fringes in the image do fade in and out.

The  $[\bar{1}20]$  SAED pattern contains strong substructure reflections, weak and diffuse satellite reflections, and streaking parallel to  $[2\bar{1}0]^*$  (Fig. 7a). The satellite reflections appear as an X with the main reflection at the intersection. The superstructure reflections occur at  $0.30 d_{2\bar{1}0}$  along  $[2\bar{1}0]^*$  and  $0.21 d_{001}$  along  $[001]^*$  (Table 9). The X of the satellite reflections intersect at an angle of  $40^\circ$ , and the spacing between the main and a satellite reflection in the X is about  $14.8 \text{ \AA}$ . The spacing between two neighboring satellite reflections in the X is about  $21.7 \text{ \AA}$ . The spacing of the satellite reflections along the  $a$  and  $c$  axes are similar to those obtained by McConnell (1962). We provide  $[\bar{1}20]$  HRTEM images from two different areas of the same crystal fragment and corresponding to the above SAED pattern



(Figs. 7b, d). Two sets of possible superstructure fringes are weakly developed and intersect at an angle of  $40^\circ$  in the upper region to form an X (arrows; Fig. 7b). The NE superstructure fringes are dominant and extend from the lower left to the middle top of the image. Within the same set, the superstructure fringes are not quite uniform in direction or separation in space. The spacing of these superstructure fringes is about  $14.8 \text{ \AA}$ . However, the FFT from the intersection area does not contain the satellite reflections that give rise to the superstructure fringes (lower-right insert). FFTs were computed for several areas (about  $5 \times 5 \text{ cm}$  in size), and most of these FFTs show the features illustrated in Figure 7c. This particular FFT is from the area above the inserted FFT (Fig. 7b). Figure 7c contains extra reflections toward the top and bottom of the FFT (arrows). These extra reflections, for example, the unit cell formed by four reflections and indicated by arrowheads, is related to the

main unit-cell by twinning. These extra “twinned” reflections are weak compared to the main reflections, and they were not observed in the SAED patterns, so they most likely formed by electron-beam transformation. It appears that the feature that causes the satellite reflections is changed by the electron beam, and gives rise to the “twin” reflections. Therefore, the satellite and “twin” reflections appear from the effect. Although the twin reflections are indicated in the FFT, the twinning is difficult to see in the HRTEM image. Figure 7d, which is from a different part of the same crystal fragment, seems to contain very weakly developed superstructure fringes, and NE-running fringes fade in and out. However, this image does not contain any twinning feature, as indicated by the FFT.

The  $[\bar{1}01]$  SAED pattern contains strong substructure reflections and weak satellite reflections (Fig. 8a). The satellite reflections are nearly parallel to  $[121]^*$ .

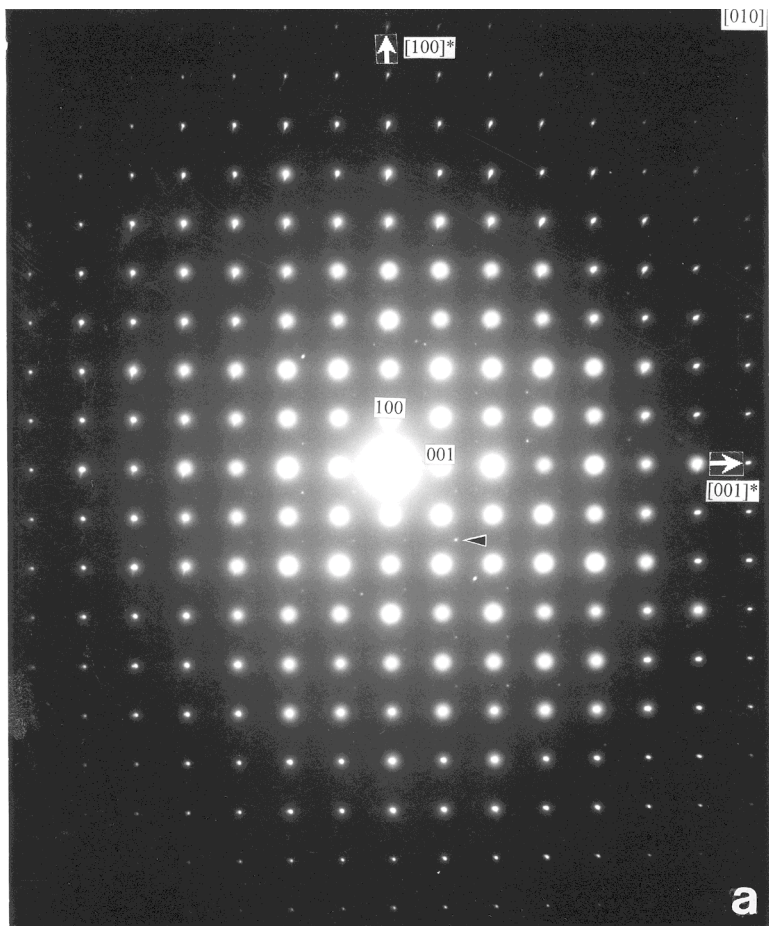
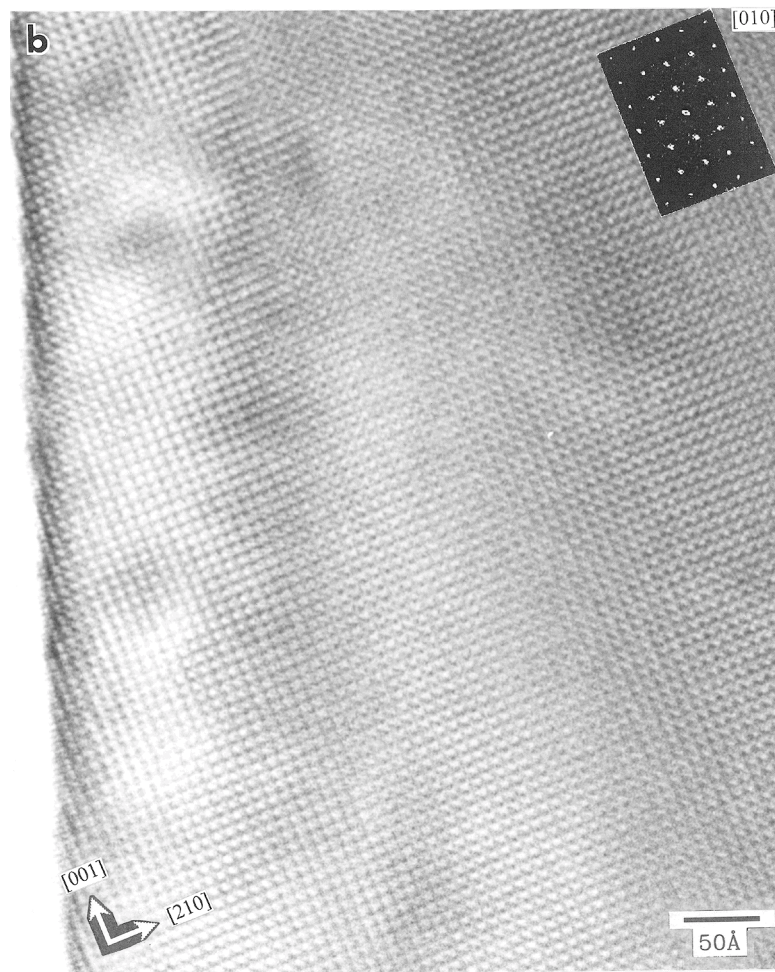


Fig. 6. a. [010] SAED pattern consisting of weak satellite reflections (*e.g.*, black arrow-head). Some additional reflections (from another crystal fragment) are also present. b. [010] HRTEM image. The NE-running fringes fade in and out. The FFT from lower region contains only the main reflections (upper-right insert).

The satellite reflections occur at  $0.5 d_{010}$  along  $[010]^*$  and  $0.32 d_{\bar{1}21}$  along  $[\bar{1}21]^*$  (Table 9). The spacing between the main reflection (M) and the satellite reflection (s), that is,  $d_{Ms}$  along  $[2\bar{1}2]^*$ , is about  $8.2 \text{ \AA}$  (Fig. 8a). The  $[\bar{1}01]$  HRTEM image, corresponding to the SAED pattern, contains possible  $d_{Ms}$  superstructure fringes as indicated by the arrow, but the FFT does not contain satellite reflections (Fig. 8b). Figure 8c is from a different area of the same crystal fragment, and it contains lattice fringes that are offset. The offset of the fringes occurs in various regions of the image. The displacement of the fringes is about one-half of the repeat unit, so these boundaries may be APBs. The vertical fringes are also offset in the upper-left region of the image. However, in this image, the possibility that the

offset of the fringes may be caused by changes in thickness of the crystal cannot be ruled out.

The SAED pattern along the  $[13\bar{2}]$  direction is shown (Fig. 9a). This pattern consists of strong substructure reflections and weak satellite reflections. The satellite reflections occur at  $0.20 d_{\bar{2}\bar{1}2}$  along  $[\bar{2}\bar{1}2]^*$  and  $0.18 d_{201}$  along  $[201]^*$  (Table 9). Along  $[\bar{2}\bar{1}2]^*$ , the satellite reflections occur in pairs, and the spacing of pairs of satellite reflections corresponds to  $16.32 \text{ \AA}$  along  $[302]$  in real space. The HRTEM image corresponding to this SAED pattern is shown (Fig. 9b). Although very weakly developed, possible superstructure fringes can be seen along the upper-left arrow; the FFT does not contain the satellite reflections. In addition, the NE-running substructure fringes fade in and out, and such fringes are



not quite straight and continuous. However, the SE-substructure fringes are straight and continuous. Offset of fringes occurs in different areas of the image and is best seen by viewing at a low angle along the lower-left arrow. The displacement of the fringes is about one-half of the repeat unit, so these boundaries may be APBs.

The  $[0\bar{1}3]$  SAED pattern consists of strong substructure reflections and weak, but well-developed satellite reflections (Fig. 10). The satellite reflections occur as pairs on either side of the main reflections. The satellite reflections occur at  $0.24 d_{\bar{1}31}$  along  $[\bar{1}21]^*$  and correspond to  $17.93 \text{ \AA}$  along  $[031]$  (Table 9). This is a one-dimensional superstructure that occurs along  $[\bar{1}21]^*$  direction. Unfortunately, no image was obtained along this direction as nepheline damages easily in the electron beam.

The  $[\bar{1}11]$  SAED pattern (Fig. 11) consists of strong substructure reflections and very weak satellite reflections that have the appearance of an X, which is similar to the satellite reflections shown in the  $[\bar{1}20]$  direction (Fig. 7a). The superstructure reflections intersect at an angle of  $40^\circ$ . The spacing between a main reflection and a satellite reflection is about  $15.9 \text{ \AA}$ . The separation between two neighboring superstructure reflections within the X is about  $23.3 \text{ \AA}$ . Streaking is parallel to  $[110]^*$ . No image was obtained along this direction.

The  $[432]$  SAED pattern consists of strong substructure reflections and complex satellite reflections (Fig. 12). The satellite reflections occur in many directions and are too complex to interpret. Streaking is also present along  $[\bar{2}23]^*$ . No image was obtained along this direction.

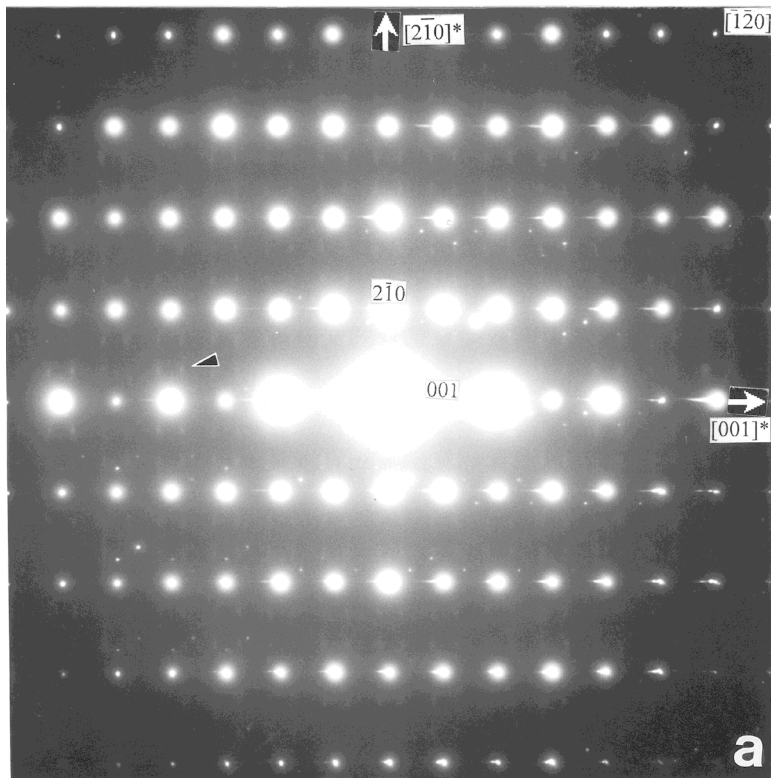


TABLE 9. THE X, Y COORDINATES OF SATELLITE REFLECTIONS AND THEIR SPACING IN THE EGAN CHUTE NEPHELINE

Fig. no.	SAED direction	Direction recip. space	Direction real space	$d_M$ mm	$d_s$ mm	$d_s/d_M$	$d_M/d_s$	$d_M$ Å	Satel. real space	
Fig. 5a	[010]	[100]*	[210]	2.40	1.10	0.4583	2.1818	8.6545	18.88	
		[001]*	[001]	2.49	0.60	0.2410	4.1500	8.3769	34.76	
Fig. 6a	$[\bar{1}\bar{2}0]$	$[2\bar{1}0]^*$	[100]	4.00	1.20	0.3000	3.3333	4.9967	16.66	
		[001]*	[001]	2.37	0.50	0.2110	4.7400	8.3769	39.71	
Fig. 7a	$[\bar{1}01]$	$[010]^*$	[120]	2.30	1.15	0.5000	2.0000	8.6545	17.31	
		$[\bar{1}\bar{2}1]^*$	[031]	4.69	1.50	0.3198	3.1267	4.2913	13.42	
Fig. 8a	$[1\bar{1}\bar{3}]$	$[201]^*$	[421]	5.10	0.90	0.1765	5.6667	3.8446	21.79	
		$[2\bar{1}\bar{2}]^*$	[302]	6.10	1.20	0.1967	5.0833	3.2099	16.32	
Fig. 9	$[0\bar{1}\bar{3}]$	$[\bar{1}\bar{2}1]^*$	[031]	4.66	1.10	0.2361	4.2364	4.2913	17.93	
Not shown	$[\bar{1}\bar{2}0]$	$[210]^*$	[540]	5.00	1.10	0.2200	4.5455	3.2711	14.87	
		[001]*	[001]	1.93	0.40	0.2073	4.8250	8.3769	40.42	
Fig. 10	$[\bar{1}\bar{1}1]$	$[110]^*$	[110]	3.82	1.30	0.3403	2.9385	4.9967	14.68	
		$[101]^*$	[211]	3.16	0.5	0.1582	6.3200	6.0191	38.04	
Fig. 11	$[4\bar{3}\bar{2}]$	Satellite reflections are complex								

$d_M$  is spacing of main reflection for planes indicated in column 3.  $d_s$  is spacing of satellite reflection. Spacing of satellite reflections in real space =  $(d_M/d_s) \times d_M$  (column 10). Satellite reflections occurring only along one direction are shown in bold. Measurements in mm were made on TEM negatives. Satel. real space: satellite reflections in real space, expressed in Å.

The satellite reflections from our nepheline specimen differ widely with respect to intensity and sharpness along different directions. In general, the satellite reflections are very weak and diffuse, indicating relatively short-range order. The spacings of the satellite reflections in our sample are summarized in Table 9. In general, the ratios of  $d_M/d_s$  are irrational numbers, so the satellite reflections in nepheline are incommensurate. The SAED patterns from the (001) plane contain no satellite reflections, so superstructure ordering in the  $a$ - $b$  plane is not attained. The satellite reflections probably arise from positional modulations of the O1 atoms.

## CONCLUSIONS

The average structure of nepheline shows that except for the O1 oxygen atom, all the other atoms in nepheline are well defined and contain no unusual features. The Al and Si atoms are fully ordered, and vacancies occur at the K site. The satellite reflections appear to arise from positional modulations of the O1 atoms.

The real structure of nepheline involves O1 atomic modulations, K-□ ordering, and Al-Si ordering. A displacive transformation occurs in nepheline at 292°C, and represents the positional modulations of all the

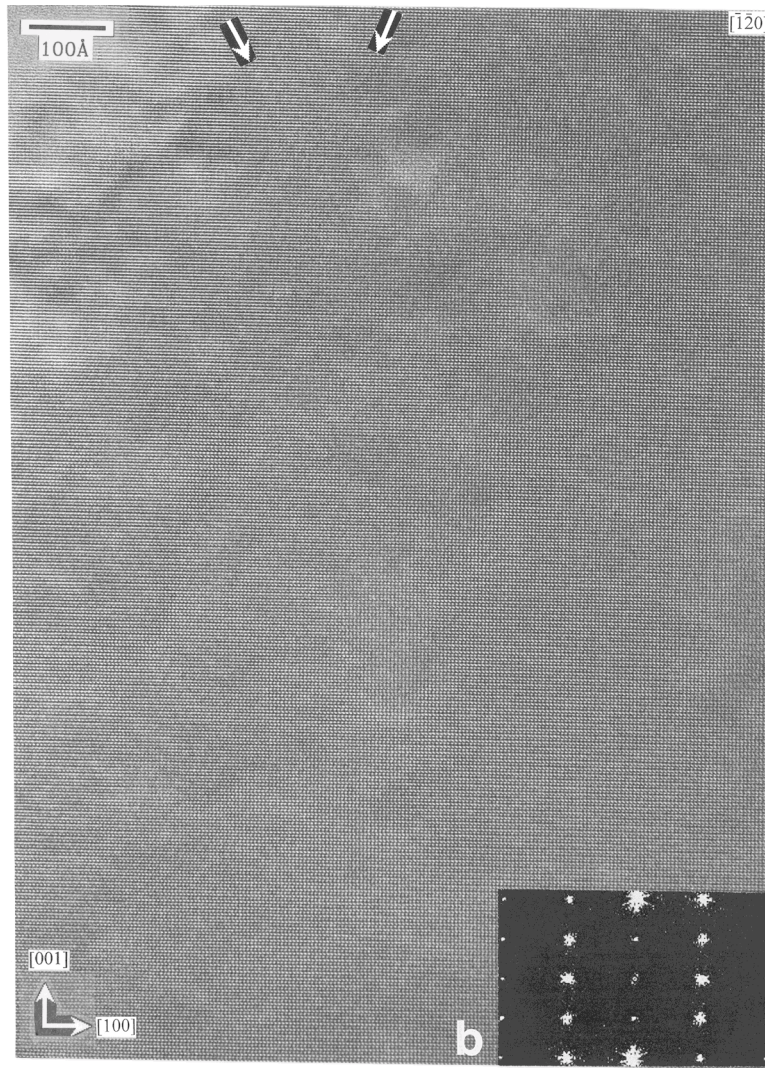


FIG. 7. a.  $[\bar{1}20]$  SAED pattern containing weak satellite reflections (*e.g.*, black arrow-head) and streaking parallel to  $[2\bar{1}0]^*$ . Some extra reflections (from another crystal fragment) are present. b.  $[\bar{1}20]$  HRTEM image. Two sets of the superstructure fringes are indicated by arrows, and they intersect in the upper region to form an X with an intersection angle of  $40^\circ$ . The spacing of these superstructure fringes is about 14.8 Å. A FFT from the intersection area only contains the main reflections (lower-right insert). c. A FFT from about a  $5 \times 5$  cm area above the lower-right insert of Figure 7b. The four arrowheads indicate the new twinned unit-cell. The orientation of the FFT is the same as that of Figure 7b. d. The  $[\bar{1}20]$  HRTEM image shows that the NE-running fringes fade in and out (arrow). A FFT from the middle region contains the main reflections (upper-left insert).

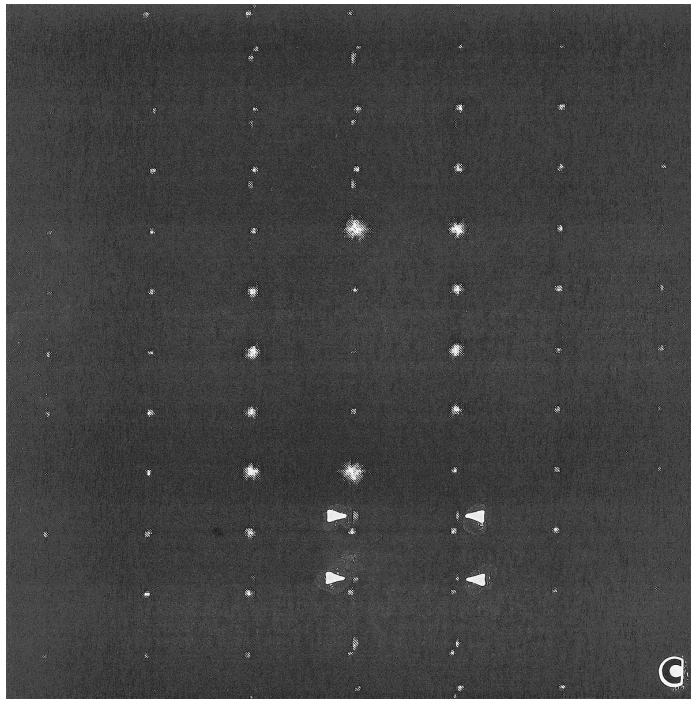


FIG. 7c

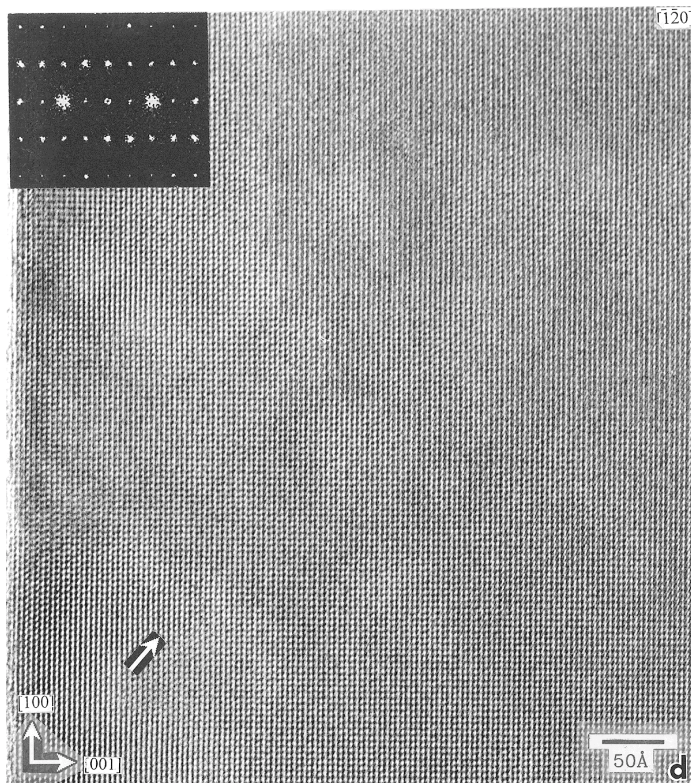


FIG. 7d

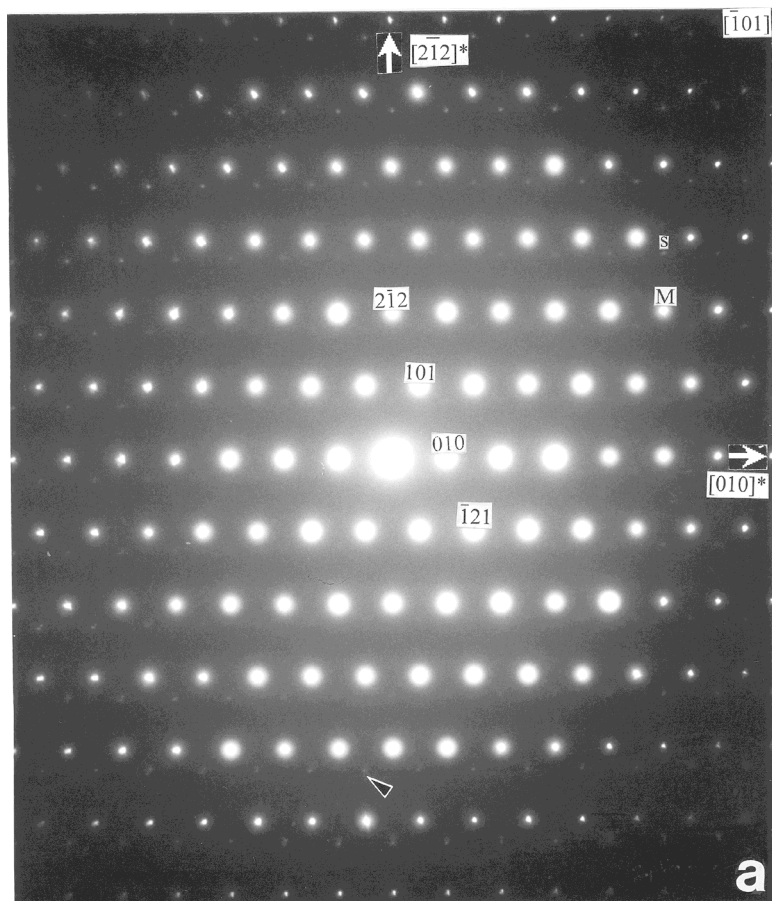


FIG. 8. a. The  $[\bar{1}01]$  SAED pattern contains weak satellite reflections (*e.g.*, black arrow-head). The spacing  $d_{Ms}$  is equal to 8.2 Å along  $[2\bar{1}2]^*$ . b. The  $[\bar{1}01]$  HRTEM image contains a few broad fringes that may be superstructure fringes (arrow). The FFT from middle-right region of the image contains the main reflections (upper-left insert). c. A  $[\bar{1}01]$  HRTEM image of nepheline. Possible APBs can be seen by viewing at a low angle along the two white arrows and along the vertical fringes in the top-left region. The FFT from the lower-left region contains the main reflections (upper-left insert), and a few reflections appear as split spots (arrow).

framework oxygen atoms, but in particular the O1 positions. This finding is consistent with the results of McConnell (1981), who documented spontaneous and reversible changes in intensity of the satellite reflections on heating and cooling at low temperatures (100–150°C).

A K–□ order–disorder transformation occurs at 399°C. This transition is consistent with the result of McConnell (1981) that indicates an irreversible change in intensity of the satellite at temperatures greater than 150°C, and is attributed to the kinetically hindered process of disordering K ions and vacancies.

An Al–Si order–disorder transformation occurs at 963°C. This transition involves the highest energy. This interpretation is consistent with the high-temperature structural results of Foreman & Peacor (1970), which show that at 900°C, the Si–O and Al–O distances are approximately equal. Our high-temperature XRD results show that nepheline melts between 1200 and 1300°C. The ordering that gives rise to the satellite reflections is destroyed in the electron beam and results in twinned unit-cells.

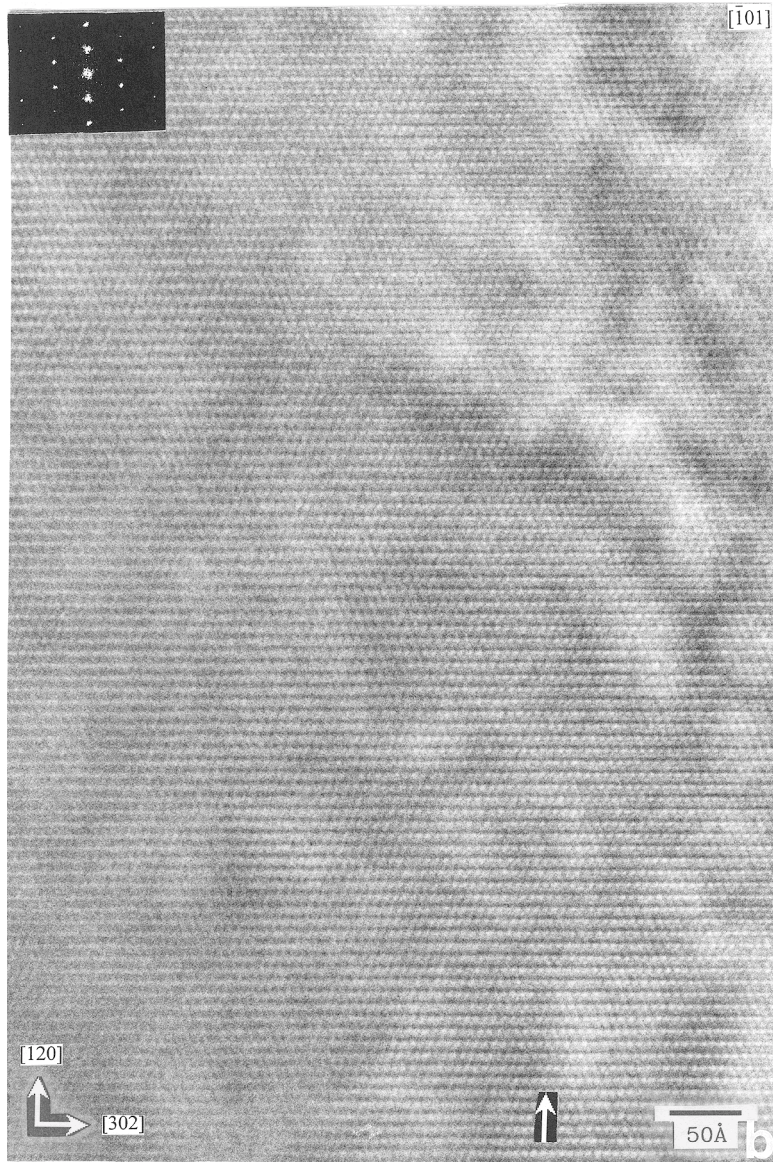


FIG. 8b

## ACKNOWLEDGEMENTS

We thank Dr. D.R. Peacor for kindly providing us with the nepheline sample used in this study, and D.H. Lindsley for his help in doing the electron-microprobe analysis, which was financially supported by a NSF grant to J.B. Parise, EAR-0125094. We thank the reviewers, Drs. E. Belluso and L. Mel'chakova and the editors, Drs. E. Sokolova and R.F. Martin for useful comments. The single-crystal XRD work was carried out in the UWI Crystallography Laboratory, which was

established with funds from UWI and the Inter-American Development Bank.

## REFERENCES

- BANNISTER, F.A. & HEY, M.H. (1931): A chemical, optical, and X-ray study of nepheline and kaliophilite. *Mineral. Mag.* **22**, 569-608.
- BUERGER, M.J., KLEIN, G.E. & DONNAY, G. (1954): Determination of the crystal structure of nepheline. *Am. Mineral.* **39**, 805-818.

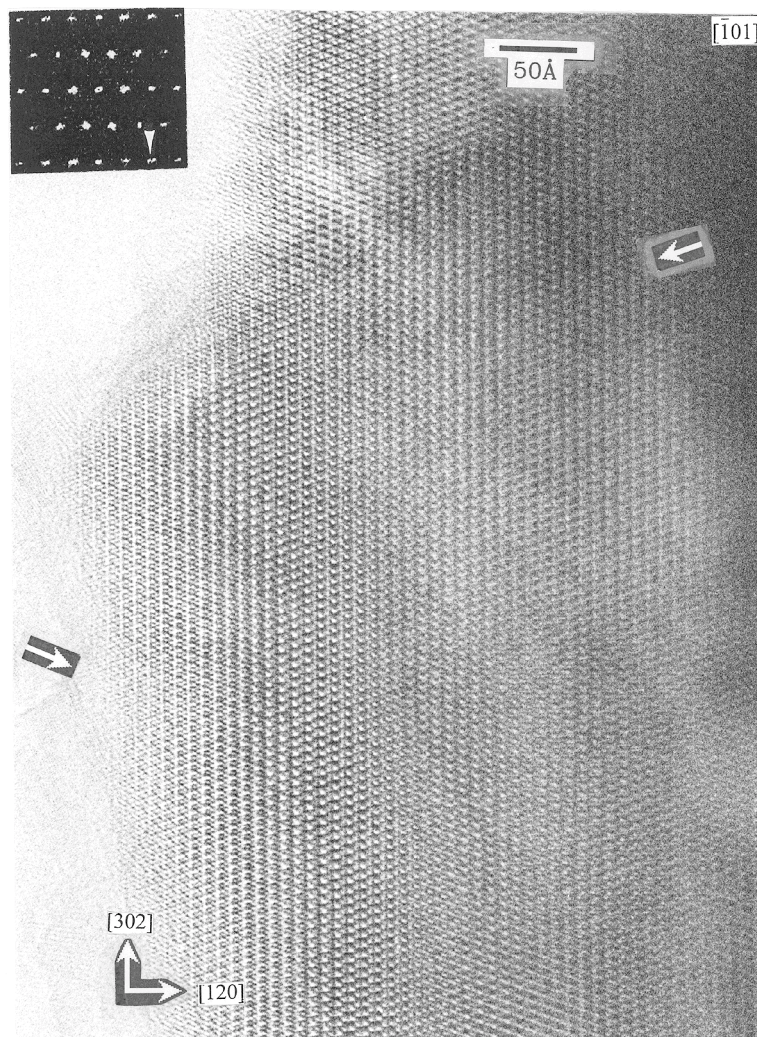


FIG. 8c

- CAPOBIANCO, C. & CARPENTER, M. (1989): Thermally induced changes in kalsilite (KAlSiO<sub>4</sub>). *Am. Mineral.* **74**, 797-811.
- CARPENTER, M.A. & CELLAI, D. (1996): Microstructures and high-temperature phase transitions in kalsilite. *Am. Mineral.* **81**, 561-584.
- DEER, W.A., HOWIE, R.A. & ZUSSMAN, J. (1992): *An Introduction to the Rock-Forming Minerals*. Longman, London, U.K.
- DOLLASE, W.A. (1970): Least-squares refinement of the structure of a plutonic nepheline. *Z. Kristallogr.* **132**, 27-44.
- \_\_\_\_\_ & PEACOR, D.R. (1971): Si-Al ordering in nephelines. *Contrib. Mineral. Petrol.* **30**, 129-134.
- \_\_\_\_\_ & THOMAS, W.M. (1978): The crystal chemistry of silica-rich, alkali-deficient nepheline. *Contrib. Mineral. Petrol.* **66**, 311-318.
- FOREMAN, N. & PEACOR, D.R. (1970): Refinement of the nepheline structure at several temperatures. *Z. Kristallogr.* **132**, 45-70.
- GREGORKIEWITZ, M. (1984): Crystal structure and Al/Si-ordering of a synthetic nepheline. *Bull. Minéral.* **107**, 499-507.
- HAHN, T. & BUERGER, M.J. (1955): The detailed structure of nepheline, KNa<sub>3</sub>Al<sub>4</sub>Si<sub>4</sub>O<sub>16</sub>. *Z. Kristallogr.* **106**, 308-338.
- HAMMOND, R.P. & BARBIER, J. (1998): Monoclinic and hexagonal nepheline structures of (Na<sub>3</sub>K<sub>1/4</sub>)AlGeO<sub>4</sub>. *Acta Crystallogr.* **B54**, 211-220.

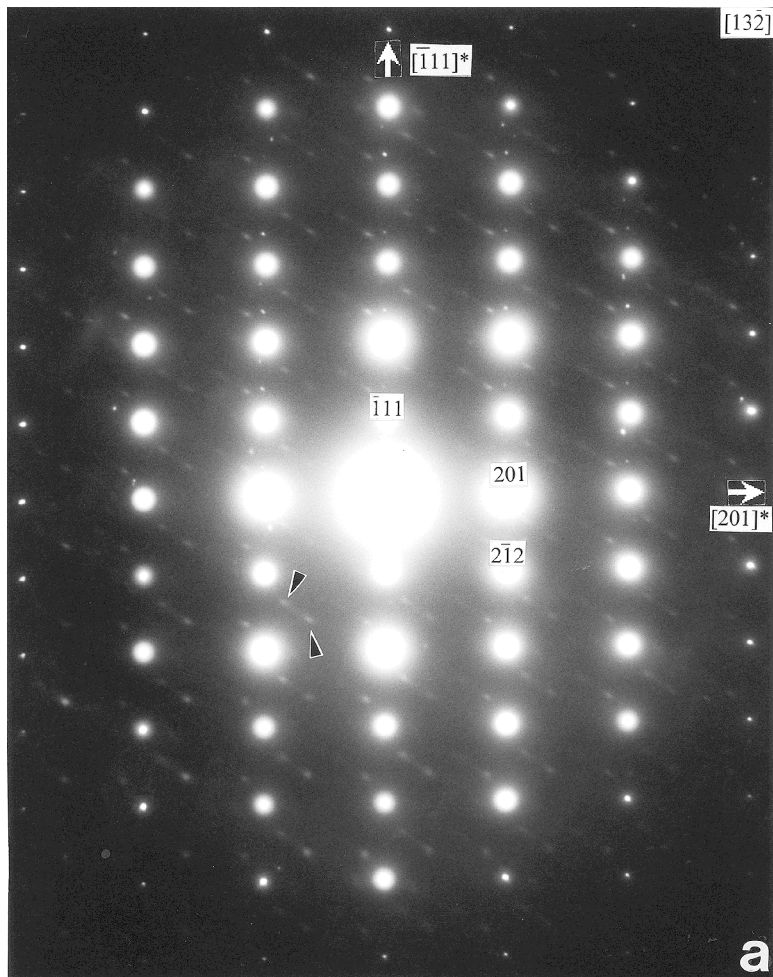


FIG. 9. a. The  $[13\bar{2}]$  SAED pattern contains weak satellite reflections (e.g., black arrowheads) and streaking parallel to  $[2\bar{1}2]^*$ . Along the  $[2\bar{1}2]^*$ , the spacing of pairs of satellite reflections correspond to 16.3 Å along  $[302]$  in real space (arrows). b. The  $[13\bar{2}]$  HRTEM image contains possible APBs in different areas of the image, which may be seen by viewing along the lower-left arrow. The top arrow indicates possible superstructure fringes that correspond to pairs of satellite reflections with a spacing of 16.32 Å. The FFT from the middle region contains the main reflections (upper-left insert).

HAYWARD, S.A., PRYDE, A.K.A., DE DOMBAL, CARPENTER, M.A. & DOVE, M.T. (2000): Rigid unit modes in disordered nepheline: a study of a displacive incommensurate phase transition. *Phys. Chem. Minerals* **27**, 285-290.

HOVIS, G.L., SPEARING, D.R., STEBBINS, J.F., ROUX, J. & CLARE, A. (1992): X-ray powder diffraction and  $^{23}\text{Na}$ ,  $^{27}\text{Al}$ , and  $^{29}\text{Si}$  MAS-NMR investigation of nepheline-kalsilite crystalline solutions. *Am. Mineral.* **77**, 19-29.

HOVMÖLLER, S. (1992): CRISP: crystallographic image processing on a personal computer. *Ultramicroscopy* **41**, 121-135.

IKOVSKIY, S.V. (1980): Type features of the composition and structural state of nepheline. *Geochem. Int.* **17**, 37-47.

LIPPMAN, E., MÄGI, M., SAMOSON, A., ENGELHARDT, G. & GRIMMER, A.-R. (1980): Structural studies of silicates by solid-state high-resolution  $^{29}\text{Si}$  NMR. *J. Am. Chem. Soc.* **102**, 4889-4893.

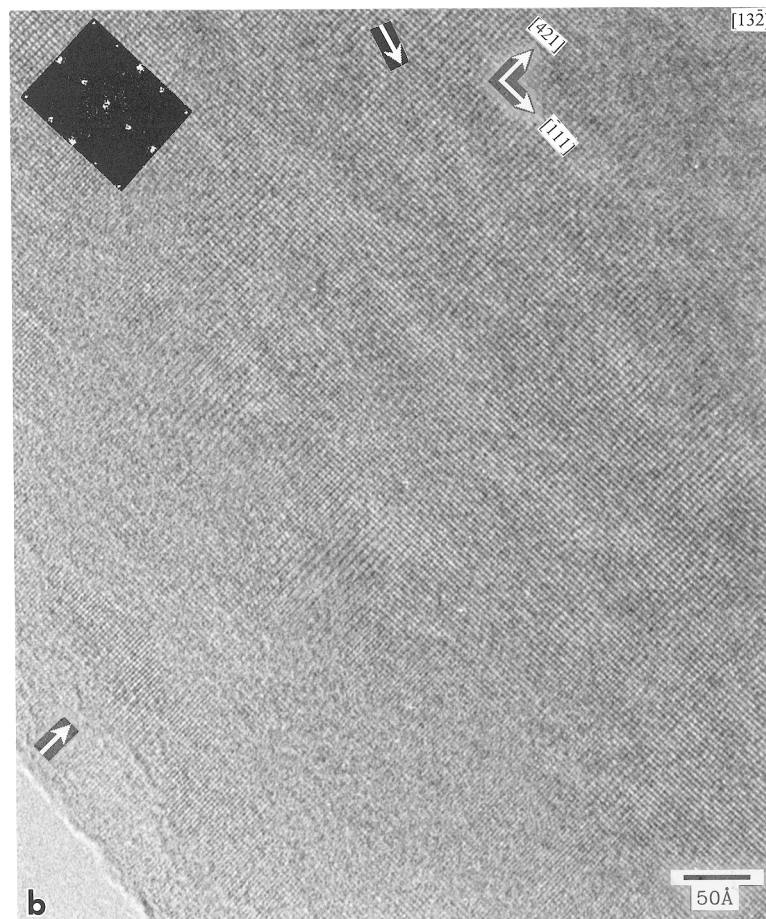


FIG. 9b

- McCONNELL, J.D.C. (1962): Electron-diffraction study of subsidiary maxima of scattered intensity in nepheline. *Mineral. Mag.* **33**, 114-124.
- \_\_\_\_\_ (1981): Time-temperature study of the intensity of satellite reflections in nepheline. *Am. Mineral.* **66**, 990-996.
- \_\_\_\_\_ (1991): Incommensurate structures. *Phil. Trans. R. Soc. London* **A334**, 425-437.
- MERLINO, S. (1984): Feldspathoids: their average and real structures. In *Feldspars and Feldspathoids* (W.L. Brown, ed.). *NATO Adv. Study Inst., Ser. C* **137**, 435-470. D. Reidel, Dordrecht, The Netherlands.
- PARKER, J.M. (1972): The domain structure of nepheline. *Z. Kristallogr.* **136**, 255-272.
- \_\_\_\_\_ & McCONNELL, J.D.C. (1971): Transformation behaviour in the mineral nepheline. *Nature* **234**, 178-179.
- SAHAMA, T.G. (1958): A complex form of natural nepheline from Iivaara, Finland. *Am. Mineral.* **43**, 165-166.
- \_\_\_\_\_ (1962): Order-disorder in natural nepheline solid solutions. *J. Petrol.* **3**, 65-81.
- SCHIEBOLD, E. (1930): Zur Struktur von Nepheline and Analcim. *Naturwiss.* **1S**, 705-706.
- SHELDRIK, G.M. (1997): SHELXL-97-1. Program for crystal structure determination. Institut für Anorg. Chemie, Univ. of Göttingen, Göttingen, Germany.
- SIMMONS, W.B., JR. & PEACOR, D.R. (1972): Refinement of the crystal structure of a volcanic nepheline. *Am. Mineral.* **57**, 1711-1719.
- SMITH, J.V. & SAHAMA, T.G. (1954): Determination of the composition of natural nephelines by an X-ray method. *Mineral. Mag.* **30**, 439-449.

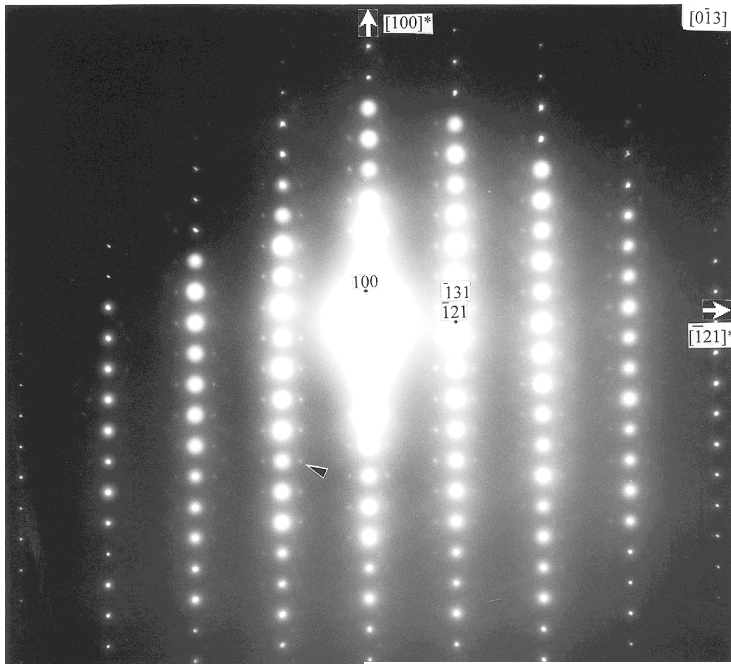


FIG. 10. The  $[0\bar{1}3]$  SAED pattern contains weak but well-developed satellite reflections (e.g., black arrowhead).

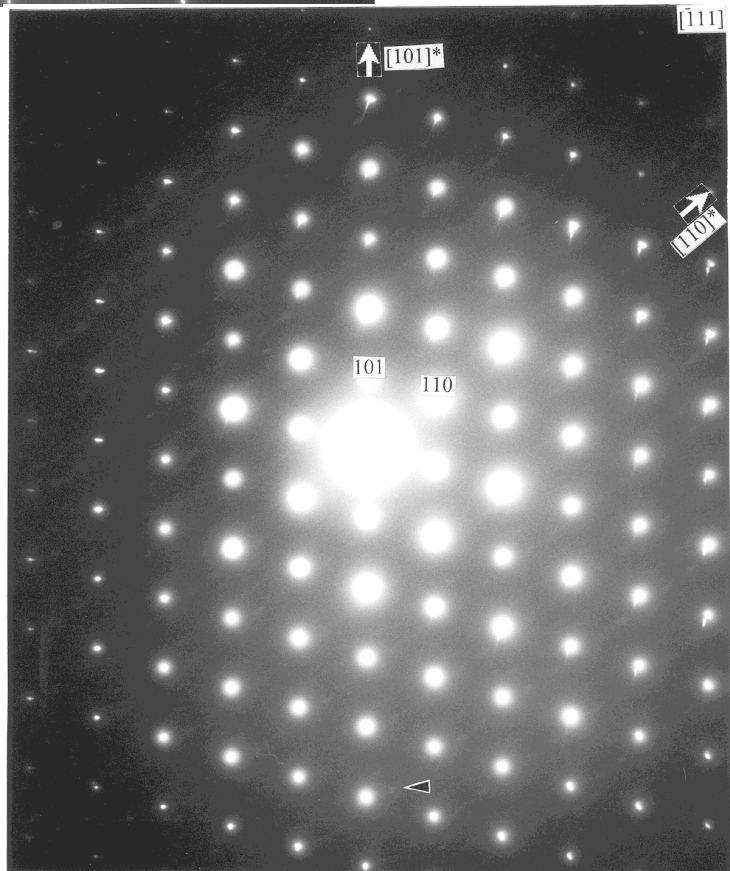


FIG. 11. The  $[\bar{1}11]$  SAED pattern contains very weak satellite reflections (e.g., black arrowhead) that have the appearance of an X. Diffuse streaking occurs parallel to  $[110]^*$ .

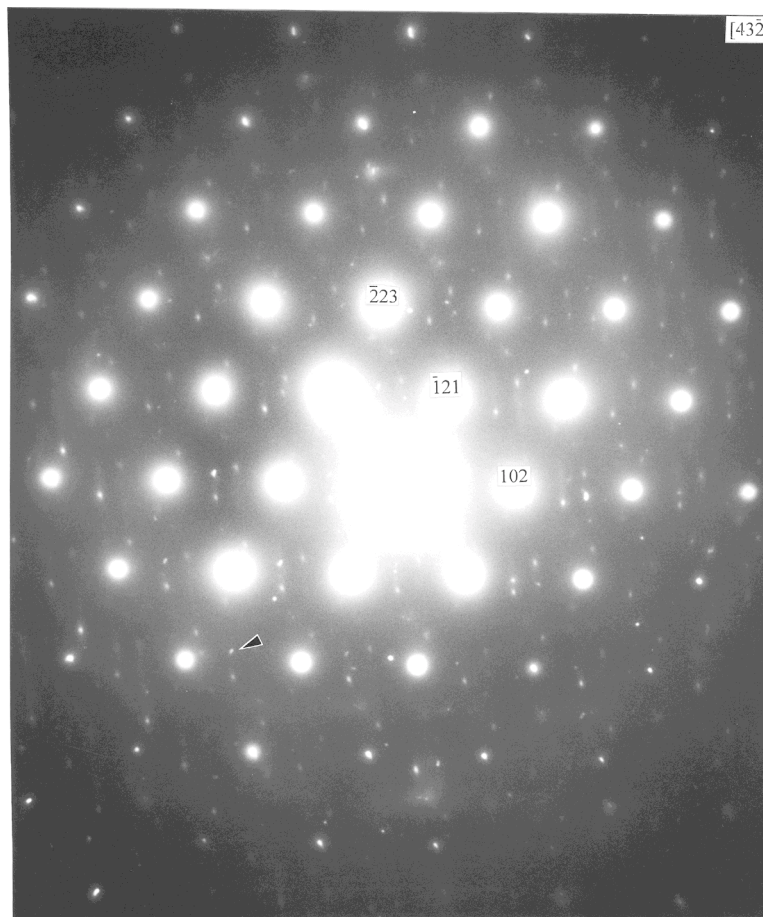


FIG. 12. The  $[4\bar{3}2]$  SAED pattern contains numerous complex satellite reflections (e.g., arrow) and streaking parallel to  $[2\bar{2}3]^*$ .

STEBBINS, J.F., MURDOCH, J.B., CARMICHAEL, I.S.E. & PINES, A. (1986): Defects and short-range order in nepheline group minerals: a silicon-29 nuclear magnetic resonance study. *Phys. Chem. Minerals* **13**, 371-381.

TAIT, K.T., SOKOLOVA, E., HAWTHORNE, F.C. & KHOMYAKOV, A.P. (2003): The crystal chemistry of nepheline. *Can. Mineral.* **41**, 61-70.

TILLEY, C.E. (1954): Nepheline – alkali feldspar paragenesis. *Am. J. Sci.* **252**, 65-75.

WILLS, A.S. & BROWN, I.D. (1999): *VaList*. CEA, France. Program available from <ftp://ftp.ill.fr/pub/dif/valist/>.

XU, HUIFANG & VELEN, D.R. (1996): Superstructures and domain structures in natural and synthetic kalsilite. *Am. Mineral.* **81**, 1360-1370.

Received July 14, 2002, revised manuscript accepted May 21, 2003.